Available online at www.sciencedirect.com
SCIENCE DIRECT®
Geochimica et Cosmochimica Acta 70 (2006) 3625–3645
Geochimica
www.elsevier.com/locate/gca

Formation and evolution of carbonate chimneys at the Lost City Hydrothermal Field

Kristin A. Ludwig [a,*], Deborah S. Kelley [a], David A. Butterfield [b], Bruce K. Nelson [c], Gretchen Früh-Green [d]

[a] University of Washington, School of Oceanography, Seattle, WA, USA
[b] University of Washington and NOAA-PMEL, Seattle, WA, USA
[c] University of Washington, Department of Earth and Space Sciences, Seattle, WA, USA
[d] Department of Earth Sciences, ETH-Zürich, Zürich, Switzerland

Received 2 September 2005; accepted in revised form 7 April 2006

Abstract

The Lost City Hydrothermal Field at 30°N, near the Mid-Atlantic Ridge, is an off-axis, moderate temperature, high-pH (9–10.8), serpentinite-hosted vent system. The field is hosted on ~1.5 Ma crust, near the summit of the Atlantis Massif. Within the field, actively venting carbonate chimneys tower up to 60 m above the seafloor, making them the tallest vent structures known. The chemistry of the chimneys and vent fluids is controlled by serpentinization reactions between seawater and underlying peridotite. Mixing of <40–91 °C calcium-rich vent fluids with seawater results in the precipitation of variable mixtures of aragonite, calcite, and brucite. The resultant deposits range from tall, graceful pinnacles to fragile flanges and delicate precipitates that grow outward from fissures in the bedrock. In this study, mineralogy, petrographic analyses, major and trace element concentrations, and Sr isotopic compositions are used to propose a model for the growth and chemical evolution of carbonate chimneys in a serpentinite-hosted environment. Our results show that nascent chimneys are characterized by a porous, interlacing network of aragonite, and brucite minerals that form extremely fragile structures. The chemistry of these young deposits is characterized by ~10 wt% Ca and up to 27 wt% Mg, extremely low trace metal concentrations, and $^{87}Sr/^{86}Sr$ isotope ratios near 0.70760. During aging of the chimneys, progressive reactions with seawater result in the dissolution of brucite, the conversion of aragonite to calcite, and infilling of pore spaces with calcite. The oldest chimneys are dominated by calcite, with bulk rock values of up to 36 wt% Ca and <1 wt% Mg. These older structures contain higher concentrations of trace metals (e.g., Mn and Ti), and have Sr isotope ratios near seawater values (0.70908). Exposed ultramafic rocks are prevalent along the Mid-Atlantic, Arctic, and Indian Ocean ridge networks and it is likely that other Lost City-type systems exist.

1. Introduction

Most submarine hydrothermal vent fields studied to date are characterized by basalt-hosted black smoker sulfide structures on or very near the ridge axis. However, studies of slow-spreading ridges have revealed that very different types of hydrothermal systems exist in association with alteration of peridotites exposed on the seafloor. Rona and others (1987) investigated serpentinite outcrops near the 15°20′ Fracture Zone at the Mid-Atlantic Ridge (MAR) and found evidence of hydrothermal activity influenced by serpentinization reactions. The later discovery of the ultramafic-hosted Logatchev (Batuyev et al., 1994; Bogdanov et al., 1995; Krasnov et al., 1995) and Rainbow (Fouquet et al., 1997) hydrothermal fields on the MAR showed that mid-ocean ridge hydrothermal vents are not exclusively basalt-hosted. Both fields support sulfide chimneys venting acidic (pH ~ 2–3), high temperature (up to 360 °C) fluids that are significantly enriched in magmatic volatiles (e.g., $CO_2 = 10–16$ mM) (Charlou et al., 2002; Douville et al., 2002). These characteristics are typical of basalt-hosted black smokers.

* Corresponding author. Fax: +1 206 543 0275.
E-mail address: kludwig@u.washington.edu (K.A. Ludwig).

0016-7037/$ - see front matter © 2006 Elsevier Inc. All rights reserved.
doi:10.1016/j.gca.2006.04.016

Both Rainbow and Logatchev fluids also contain elevated concentrations of H_2 (12–16 mM) and CH_4 (2.1–2.5 mM), which are indicative of subsurface serpentinization reactions (Gracia et al., 2000; Charlou et al., 2002; Douville et al., 2002; Seyfried et al., 2004). More recent investigations of the Arctic and Indian Ocean ridge systems show that venting from peridotite-rich environments may be widespread (e.g. Bach et al., 2002; Edmonds et al., 2003; Baker et al., 2004).

Compared to other studied sites, the Lost City Hydrothermal Field (LCHF) is an extreme endmember in which hydrothermal geochemistry is controlled primarily by serpentinization reactions that produce pH 9–11, <40–91 °C fluids enriched in H_2 (up to 15 mmol/kg) and CH_4 (1–2 mmol/kg), with ≪1 mmol/kg of CO_2 (Kelley et al., 2005; Proskurowski et al., 2006). These fluids are low in most metals and silica and are enriched in calcium (up to ~30 mmol/kg). Mixing of these fluids with seawater results in the precipitation of large carbonate chimneys. Results presented in this study provide the first detailed examination of the geologic, tectonic, and chemical processes that produce and influence the Lost City carbonate structures over time.

2. Methods

2.1. Field sampling

Carbonate chimney, fissure-filling material, and fluid samples were collected across the LCHF (Fig. 1) during two cruises in 2000 and 2003 (Kelley et al., 2001, 2005). Seven carbonate samples and three vent fluid samples were collected when the field was discovered in late 2000. The 2003 expedition (see http://www.lostcity.washington.edu) recovered >100 carbonate and basement rock samples. A representative set of 32 carbonate samples were analyzed in this study; this set includes 11 actively venting structures, 13 inactive deposits, and 8 fissure samples (Fig. 1 and Table 1). Due to poor navigation, samples collected during dive 3880 are not included in Fig. 1. In addition to the bulk rock analyses, transects across two separate structures were analyzed for major and trace elements. Subsamples across the ~20 cm-wide base of chimney 3881-1338 were taken every ~2.5 cm. Subsamples across a basal transect of chimney 3651-0938 were taken every ~1 cm across a ~16 cm wide slab.

Fluid samples were collected during ALVIN dives using standard titanium major and gas-tight samplers. A hydrothermal fluid particulate sampler (HFPS) was also used to collect multiple filtered and unfiltered vent fluid samples during four dives.

2.2. Analytical methods

Mineralogy was determined by powder X-ray diffraction (XRD) at the University of Washington (UW) and ETH-Zurich (ETHZ). Twenty-one polished thin sections of carbonate chimney samples were used to characterize texture, mineralogy, and crystal growth patterns with a petrographic microscope. Porosity was determined using ®Metamorph image processing software.

Concentrations of major cations (Na, K, Mg, and Ca) in the carbonate and fluid samples were measured at the Pacific Marine Environmental Laboratories of the National Oceanographic and Atmospheric Administration (PMEL-NOAA) in Washington. Subsamples of digested carbonate samples were diluted 100-fold by mass and analyzed using a Dionex DX500 ion chromatograph with a precision of 2% (2-sigma). Carbonate Fe and Sr concentrations were determined using a Perkin-Elmer 5000 flame atomic absorption (AA) spectrophotometer at the UW. Iron concentrations were all below detection limit (50 ppm). Fluid Sr concentrations were determined using the same instrument, with a precision of 4%.

Carbonate chimney and fissure samples were analyzed for trace element concentrations with a Perkin-Elmer ICP-MS at the UW. After hand-crushing, foraminifera, shell, and lithic fragments were removed from each sample prior to processing to minimize contamination by foreign materials. Samples were digested following a modified procedure after Morford and Emerson (1999). Carbonate samples were analyzed for Ti, V, Cr, Mn, Ni, Co, Cu, Zn, Mo, Ba, Pb, and U by ICP-MS using a standard curve technique with $CaCO_3$ matrix-matched standards. A spiked calcium carbonate reference material was analyzed as a control to determine instrument accuracy and precision and to account for matrix effects. The calcium carbonate standard was made from 99.999% pure (Aesar) $CaCO_3$ digested and spiked with 10 ppb of each analyte (Specpure ICP standards, Alfa-Aesar). Zn and Pb concentrations were not determinable due to matrix effects with Ca. Titanium concentrations were also difficult to resolve due to matrix effects. The accuracy, precision, and detection limits for each analyte are listed in Table 2b.

Seven carbonate rocks, thirteen vent fluids, and two background seawater samples were analyzed for Sr isotope ratios by thermal ionization mass spectrometry at the UW and at ETH-Zurich, using methods described by Nelson (1995). Two replicates of all rock samples and three fluid samples were measured for reproducibility and compared to known values of International Association of Physical Sciences Organizations (IAPSO) standard seawater. At the UW, the average $^{87}Sr/^{86}Sr$ of the NBS987 standard measured during the period of analyses was 0.710283 with a 2-sigma standard deviation of 40 ppm ($N = 6$). The average $^{87}Sr/^{86}Sr$ of the NBS987 standard measured at ETHZ was 0.710204 with a 2-sigma standard deviation of 26 ppm ($N = 10$). These values lie well within long-term average values for the standards. All Sr isotope ratios were normalized to $^{86}Sr/^{88}Sr = 0.1194$ and to $^{87}Sr/^{86}Sr = 0.71024$ of NBS 987.

3. Geologic setting

The LCHF is located ~15 km west of the axis of the MAR at 30 °N (Kelley et al., 2001) (Fig. 1) at a water depth of ~750–850 m near the summit of the Atlantis Massif. This mountain is a ~3800 m-tall, inside corner high that has been exposed by low-angle detachment faulting; crust in this area is ~1–2 Ma (Cann et al., 1997; Blackman et al., 1998; Kelley et al., 2001; Blackman et al., 2002; Schroeder and John, 2004; Karson et al., 2006). The massif is composed of variably deformed and serpentinized harzburgitic peridotite and gabbroic material (Blackman et al., 1998; Kelley et al., 2001; Blackman et al., 2002; Früh-Green et al., 2003; Kelley et al., 2005; IODP Expedition Scientific Party, 2005a,b). Although seismic surveys across the massif suggest active serpentinization to depths of 500 m, with potentially fresh peridotites below this zone (Canales et al., 2004), results from IODP Legs 304 and 305 point to significant gabbroic bodies within the massif (IODP Expedition Scientific Party, 2005a,b). The seismically active, 75 km-long Atlantis Transform Fault (ATF) bounds the southern face of the massif (Smith et al., 2003), which contains significant exposures of serpentinite with lesser gabbro (Blackman et al., 2002; Boschi et al., 2006; Karson et al., 2006). The complex fault networks

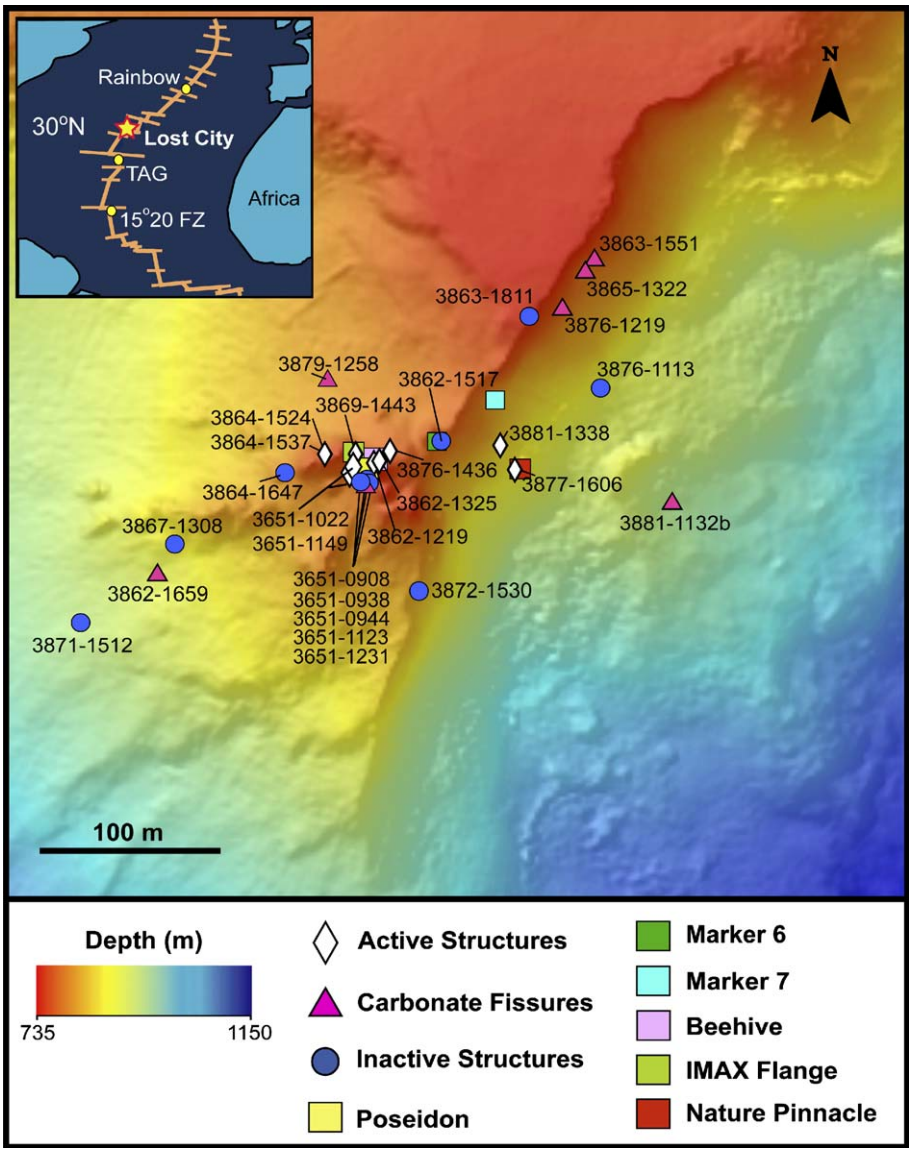

Fig. 1. The Atlantis Massif is located approximately 15 km west of the spreading axis of the Mid-Atlantic Ridge. The Lost City Field is located on the southern face of the massif on variably altered and deformed mantle rocks with lesser gabbroic material that is ~1.5 my in age (Blackman et al., 2002). The massif rises from a water depth of ~6000 m to ~700 m over a horizontal distance of ~20 km. Markers denote specific features within the field. Locations of most carbonate samples examined in this study are classified (active, inactive, fissure) based on field observations. Samples 3873-1233 and 3881-1338 are beyond the western and southern boundaries of this map, respectively.

associated with this environment play an important role in focusing and sustaining hydrothermal circulation within the massif (Kelley et al., 2005).

3.1. The Lost City Hydrothermal Field

Hydrothermal activity is concentrated at the southern edge of the Atlantis Massif on a down-dropped promontory (Kelley et al., 2001; Früh-Green et al., 2003; Kelley et al., 2005). Within the field and in the surrounding areas, "active," "inactive," and "fissure-filling" carbonate formations are observed (Fig. 1). Most of the carbonate structures grow directly from serpentinite bedrock (Fig. 2a). Splintered debris and talus of extinct chimneys surround the base of several of the large structures (Fig. 3) and accumulate on the slope or in saddles between chimneys. Fluid percolation through extinct carbonate deposits and talus forms cross-cutting veins and small chimneys, and leads to variable cementation of the carbonate talus. Diffuse venting occurs from numerous chimneys and flange deposits within the core of the field (Fig. 2). Radiocarbon isotopic analyses on a subset of active and inactive chimneys and vein material collected in 2000 indicate that hydrothermal activity has spanned at least 30,000 years (Früh-Green et al., 2003) (Table 1).

3.2. Active structures

Actively venting chimneys within the LCHF emit 40–91 °C fluids and range in size from fledgling, <1 m tall

Table 1
Mineralogy and petrography of Lost City carbonate samples

Sample ID[a]	Type[b]	Location	Depth[c]	Temp[d]	Hand sample description	Mineralogy[e]	^{14}C Age[f]	Porosity[g]	Stage
3651-1022	A	Top of Poseidon	731	75	White cauliflower formation, friable	arag, bru	50 ± 45		II
3651-1149	A	IMAX flange	792	55	Bright white, fragile	arag, bru	195 ± 45		II/III
3862-1219	A	Poseidon, S side	730	59	White tower	arag, bru, ±cc, ik?	34.3	III	
3862-1325	A	Poseidon, S spire	733	59	Cream/bright white tower	arag, bru, ±cc		56.7	III
3864-1524	A	IMAX flange edge (front)	764	53.5	Bright white, fragile	arag, bru, cc, ik?			II
3864-1537	A	IMAX flange edge (left)	764	53.5	Bright white, friable, quill-shaped flow channels	arag, bru, cc, ik?			II
3869-1443	A	Marker C, spire above flange	780	9.4	Reddish discoloration, cream-white with meringue-like texture	arag, bru, cc		33.0	II/III
3869-1446	A	Marker C, flange	780	9.4	Reddish discoloration, friable, rough texture with visible blades of aragonite	arag, bru, cc			II
3876-1436	A	Beehive	746	91	Ivory color, feathery texture	arag, bru, cc			II
3877-1606	A	Near Nature Tower, small chimney on 30m tall active structure	841	62	Bright white, friable, quill-shaped flow channels, filaments on surface	arag, bru, cc			II/III
3880-1532	A	Below Nature Tower	845		White, very friable, filaments	arag, bru, cc			II
3651-0908	I	Base of Poseidon, S face	844		Dark brown exterior, well-lithified, fossils	cc, high-Mg cc	25120 ± 210		V
3651-0938	I	Poseidon, S face	786		Intact chimney, dark exterior, ivory interior, well-lithified, fossils	arag, cc	11820 ± 85		V
3651-1123	I	W of IMAX flange in saddle	799		Gray exterior, well-lithified	arag	970 ± 35		IV/V
3651-1231	I	Top of Poseidon, in saddle	731		Gray exterior, white interior mottled surface, well-lithified,	arag, cc	585 ± 35		IV/V
3862-1517bs[h]	I	Marker 6	777		Gray exterior, ribbon-like texture	arag, cc		36.2	IV
3862-1517tp[h]	I	Marker 6	777		Gray exterior, ribbon-like texture				III
3863-1811	I	Low area N of Poseidon	787		Resembles natural concrete in texture & color, fossils	arag, cc		7.4	V
3864-1647	I	Below Marker 1	805		Dark, weathered rind, well-lithified, flow channels preserved, fossils	arag, cc		25.2	IV
3867-1308	I	W part of main field, below Poseidon?	851		Dark gray spire, bright white interior, fossils	cc, bru		12.9	IV/V
3871-1512	I	Below W part of vent field	911		Dark brown/black exterior, bright white interior, exterior had abundant biological growth	arag, cc			V

Sample ID	Type	Location	Depth	Temp	Hand sample description	Mineralogy	C Age	Porosity	Stage
3872-1530	I	Talus below main field	819	9.9	Ivory color, coarse-grained carbonate, well-lithified	arag, cc, talc, serp		III/IV	
3873-1233	I	Talus, W of main field	956		Dark brown exterior, massive, vuggy texture, contains frags of basement rock and fossils	cc			V
3876-1113	I	E part of field, on serpentinite basement	872		Gray, fossils, fluid channels visible, coral on exterior	arag, bru, cc			IV/V
3881-1338	I	Nature Tower	855		95cm tall intact spire, mostly white, sections of pistachio green interior (points 2, 3), H_2S smell, recently active?	arag, bru, cc			III
3651-0944	F	Face of Poseidon	785		Growing out of cc crust, H_2S smell upon recovery; poss. recently active	arag, bru, cc	300 ± 35		I/III
3862-1659	F	btwn Marker 1 and Marker 4	755		Carbonate fissure cross-cutting carbonate	arag, bru, cc		53.9	I
3863-1551	F	serpentinite wall, E part of field	768		Delicate carbonate fissure	arag, bru, cc		37.4	I/II
3865-1322	F	near Marker 7, on top of carbonate cap	742		Growing out of crack in cap, flow channels evident, rec. active?	arag, bru, cc		35.5	I/III
3876-1219	F	serpentinite wall, E part of field	799		Mottled dark exterior, with embedded oxidized serp., relict fluid channels visible	arag, bru, cc			I/III
3879-1258	F	serpentinite wall, S of Nature Tower	847		Mottled brown/cream exterior, ivory interior, some flow channels visible	arag, bru, cc			I/IV
3880-1353	F	serpentinite wall, SW of Marker 7	818		Cream white, mottled, relict flow channels visible, shells, fossils	arag, cc			I/IV
3881-1132b	F	serpentinite wall, E part of field	822		Dark cream color, friable, swirled, sub-vertical flow channels, some in-filled with brucite, poss. recently active	arag, bru, cc			I/III

[a] Samples beginning with 3651 from 2000, samples beginning with 3862 through 3881 are from 2003 cruise.
[b] A, actively venting structure; I, inactive structure; F, carbonate growing from fissure in serpentinite bedrock unless otherwise noted; categories based on field observations.
[c] Depth in meters.
[d] Temp indicates temperature in °C of fluid flowing from where sample was collected. Inactive samples were at ambient water temperature (~7 °C).
[e] Mineralogy abbreviations: arag, aragonite; cc, calcium carbonate; bru, brucite; ik, ikaite; serp., serpentine.
[f] ^{14}C age reported in years, from Früh-Green et al. (2003).
[g] Porosity reported in percent (determined using thin sections).

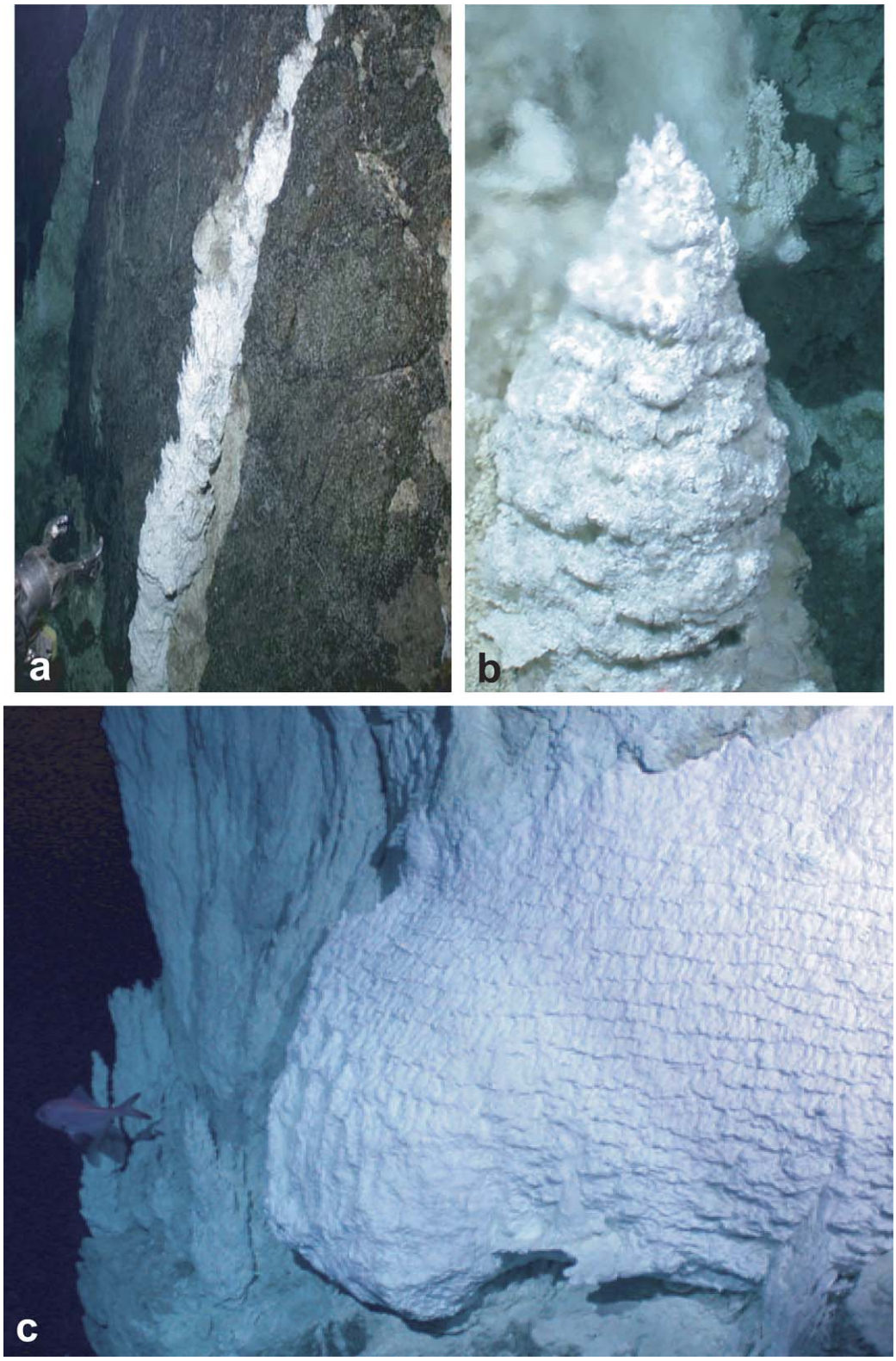

Fig. 2. Fissure-filling deposits and actively venting structures at Lost City. (a) Carbonate forms in a fissure in serpentinite bedrock on the east side of the field. (b) The 80 cm-tall Beehive structure emits pH 10.7 shimmering fluids at 91 °C. (c) A diffusely venting shingled wall of carbonate on the north face of the Nature Tower; a 30 m tall edifice on the east side of the field. The wreck fish in the left portion of the photo is approximately 1 m in length.

structures to mature chimneys that grow up to 60 m in height. The bases and significant portions of some of the larger active structures are well lithified. These sections grade upward and outward into more porous carbonate where diffuse venting is concentrated (Fig. 2b). The actively venting structures are characteristically snow white, friable,

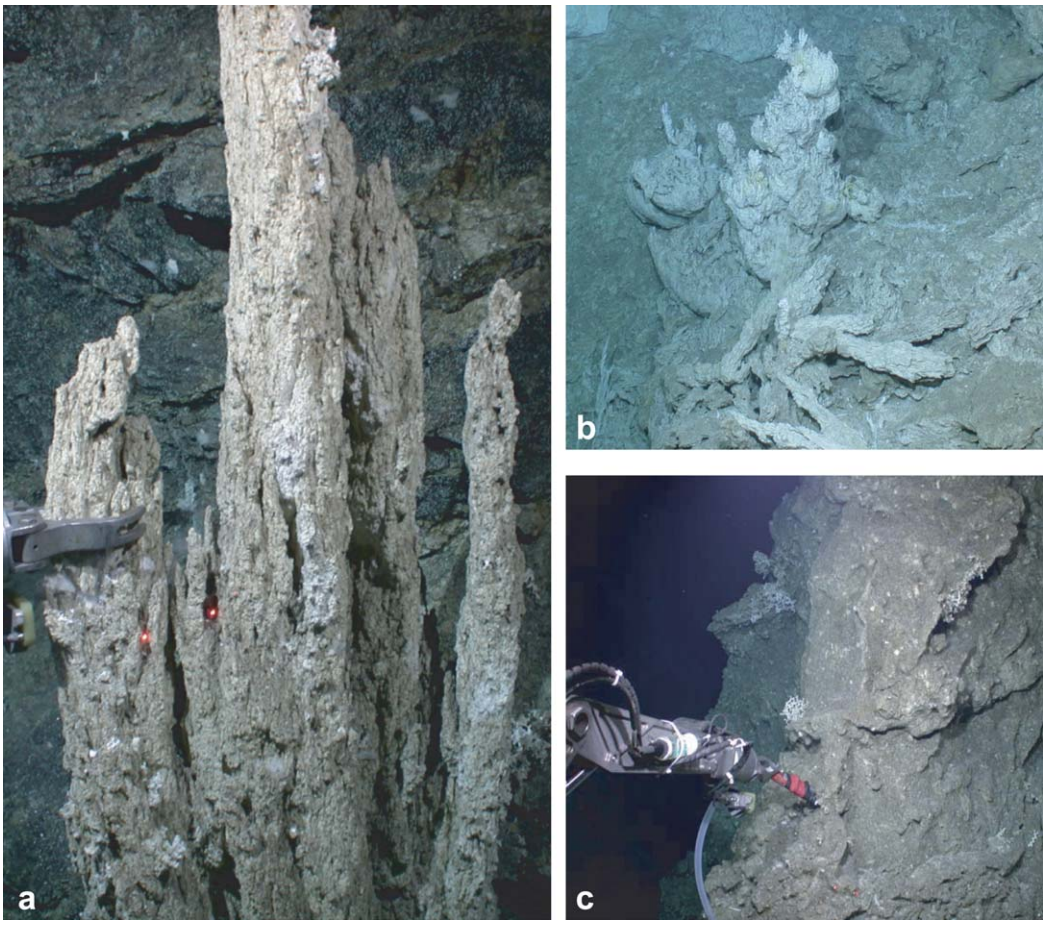

Fig. 3. Inactive structures at Lost City. (a) Inactive chimney composed of well-lithified carbonate with a dark brown, pitted exterior, and white interior. The two red laser points shown from the submersible Alvin are 10 cm apart. (b) Tumbled, inactive chimney debris form a talus pile on the south east corner of the Poseidon edifice. (c) Dark, knobby exterior walls populated by worms and deep sea corals characterize old, inactive structures.

and porous (Table 1). However, some of the actively venting carbonate material is significantly discolored bright orange-red or pale pistachio green on both the exterior and interior of the structures. The cause of these discolorations remains unexplained, but may reflect biological influences.

The central landmark in the field is Poseidon, which is the largest of the edifices (Fig. 1) (Kelley et al., 2001, 2005). This gigantic pillar towers 60 m above the seafloor and is 15 m in diameter at its top where fluids vent at temperatures up to 80 °C. Most of its base is composed of massive carbonate with several buttresses resembling "drapery" formations commonly observed in caves. These basal structures are likely relict carbonate formations that have melded together. Crisscrossed networks of younger carbonate veins cut through the massive structures, indicating complicated fracture-fill processes that are important in the long-term outward growth of the chimneys.

Many of the large edifices host parasitic growths that include 1–2 m wide flanges and delicate carbonate cones, which grow up to 10 m in height. Flanges such as the IMAX flange trap pools of reflective, warm (up to ~55 °C) vent fluids. Carbonate cone or "beehive"-shaped deposits (Fig. 2b) are morphologically similar to young black smokers (Delaney et al., 1992; Fouquet et al., 1993; Hannington et al., 1995). Typically their outer surfaces are bright white and have a rippled, shingled appearance (Fig. 2c). Some of the beehive structures form on the tops of flanges, others are sub-horizontal parasitic growths on larger chimneys. The "Beehive" structure on Poseidon vents the highest temperature fluids measured at Lost City (91.4 °C).

Hand samples of the most active portions of the structures exhibit delicate, elongated quill-like crystals of carbonate, very fine splinters of aragonite, and pockets of brucite. Upon recovery, many of the active samples appeared to dissolve and leaked a cloudy white fluid. This observation indicates that some of the samples may contain the mineral ikaite ($CaCO_3{\cdot}6H_2O$), a hydrous, unstable form of calcium carbonate that rapidly decomposes at room temperature and pressure (Marland, 1975; Bischoff et al., 1993a; Buchardt et al., 2001; Kelley et al., 2005). Many of the samples from the IMAX flange exhibited characteristics of ikaite.

3.3. Fissure deposits

A second class of carbonate structures at the LCHF is "fissure" deposits. Throughout the field, the steep serpentinite walls of the massif are cut by several cm-wide fractures or fissures filled with carbonate (e.g., samples 3863-1551 and 3881-1132b) (Table 1 and Fig. 2a). There are also cross-cutting, in-filled fractures in both the carbonate cap and in the faces of large carbonate structures such as Poseidon (e.g., samples 3865-1322 and 3862-1659, respectively) (Table 1). Collectively, these fracture-filling carbonates are categorized as fissure deposits in this study. Active venting was rarely observed at any of these sites. The fissure deposits are typically cream white with relict fluid flow paths defined by sinuous carbonate bounding pore space (Table 1).

3.4. Inactive structures

Inactive structures are carbonate deposits that were clearly not venting at the time of sampling. The morphology of the inactive structures varies from textures and shapes similar to those found in the active chimneys, to structures in which very little delicate morphology is preserved (Table 1). There are several types of inactive chimneys. These include structures that were not actively venting at the time of sampling, but may have been "recently active" based on their light color, delicate morphology and geochemical composition (e.g., 3881-1338, described below). Structures such as 3862-1517, are inactive but still retain significant porosity (up to ~35%), are ivory in color, and display well-defined fluid flow paths. Finally, some of the chimneys have been clearly inactive for some time (e.g., 3651-0908). These chimneys are characterized by their dark gray, brown, or black exterior, and white, ivory, or gray interior. The outer walls and rinds of these older structures are characteristically rough and pitted or knobby in texture and are colonized by corals and worms (Fig. 3). These formations are typically massive and extremely well-lithified and little evidence remains of the original conduits for fluid flow.

4. Results

4.1. Vent structure mineralogy and petrography

In contrast to the diverse mineral suites that typify black smoker chimneys, the mineralogy of the Lost City deposits is simple. Active carbonate structures are predominantly composed of aragonite, calcite, and brucite (Table 1). Calcite, minor brucite, and variable amounts of aragonite dominate inactive chimneys. Texture-porosity-mineralogical relationships can be grouped into five general categories (Figs. 4 and 5):

i. >50% porosity, fluid-flow paths defined by direction of crystal growth, aragonite-dominated, fragile.
ii. 30–50% porosity, flow paths well defined and some are lined with brucite; rock is a mixture of aragonite, brucite, with some calcite.
iii. 10–30% porosity, flow paths are well defined but some channels have been filled with calcite, rock is a mixture of aragonite, brucite, and calcite.
iv. 5–10% porosity, relict flow channels still discernable, some fossils in outer walls, calcite-dominated.
v. <5% porosity, massive, no evidence of flow channels, absence of brucite, fossil-rich, calcite-dominated rock, extensive recrystallization.

In young, actively venting flanges, nascent fluid flow channels form between blades of aragonite (Fig. 4a). In more mature, but still active chimneys, sinuous flow paths are well-formed (Fig. 4b) and aragonite, brucite, and calcite are present within the structures. In older deposits that are no longer venting, microchannels are progressively in-filled with micritic calcite and only trace brucite remains (Fig. 4c). In well-lithified structures, marine fossils are incorporated into the chimney walls (Fig. 4d). These fossils include shells of planktonic marine foraminifera, gastropods, echinoderm spines, sponge spicules, and pteropods.

4.2. Major elements

Bulk rock chemistry reflects the mineralogical transformations associated with temporal evolution of the chimneys. All samples (active, inactive, and fissures) have variable concentrations of Mg and Ca (Table 2a and Fig. 5), and comparatively low concentrations of Na and K (~<1 wt% Na + K) (Table 2a). The active chimneys have average Ca and Mg concentrations of ~19.1 wt% and 14.6 wt%, respectively. In contrast, the inactive structures generally contain more Ca, with an average of 29.1 wt% Ca and <5.0 wt% Mg (average 3.9 wt%). Calcium and Mg concentrations of carbonate material growing out of fissures are similar to inactive structures, with average values of 24.2 wt% and 9.4 wt%, respectively. No trends in Na and K concentrations were observed when comparing active, inactive, and fissure structures.

4.3. Trace elements

Although the carbonate mineralogy and major element chemistry document diagenetic changes in the structures and distinct differences between active, fissure, and inactive carbonate deposits, few trace elements complement these trends (Table 2b). In general, the active structures have extremely low (and commonly below detection limit) concentrations of most trace elements, while inactive chimneys exhibit elevated concentrations of many of the transition metals.

Copper, Ba, and U show variable concentrations in active, fissure, and inactive structures, with concentrations of up to 1.24 ppm Cu, 0.70–54 ppm Ba, and 0.30–11 ppm U

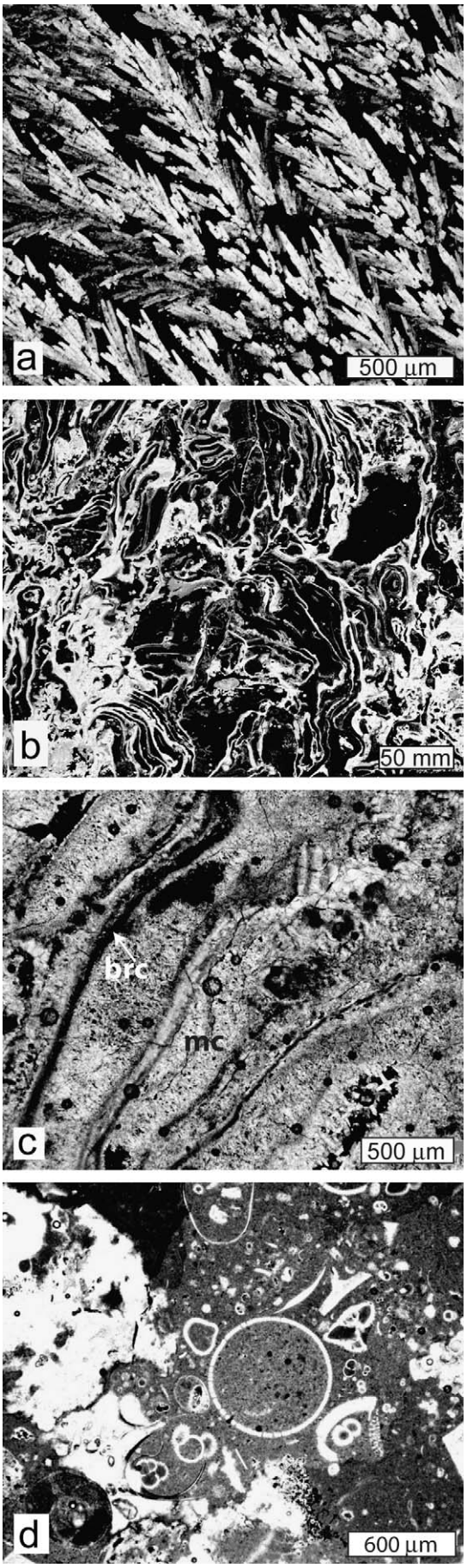

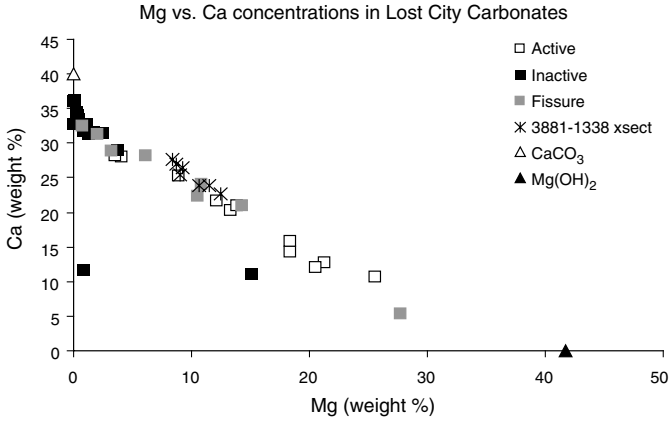

Fig. 5. Magnesium and calcium concentrations in bulk rock carbonate samples from structures at the Lost City Hydrothermal Field. Concentrations of Ca and Mg in calcium carbonate ($CaCO_3$) and brucite [$Mg(OH)_2$] are shown for comparison. Samples are categorized as active, inactive, and fissure (see Section 3 for details). Samples from chimney 3881-1338 are collected from a basal transect: although this chimney was not venting at the time of collection, it shares some morphological and geochemical traits with some of the active chimneys and may have been recently venting.

(Table 2b). There is no clear relationship between structure type and trace metal concentration. However, on a smaller scale, across the basal transect of sample 3881-1338, which may have been recently active, there is a positive correlation between Sr, U, and Ba (Table 2b and Fig. 6a). Trends across this transect are asymmetric. Sr increases from 326 ppm at Point 2 to 2222–2800 ppm towards the exterior (Fig. 6a). Ba increases from 0.14 ppm to 16.70–28.73 ppm at the outer margins (Fig. 6a). The correlation between Sr and U is not as strong, although U concentrations increase slightly from 0.97 ppm in the interior to 2.2 ppm towards the exterior (Fig. 6a). In contrast, similar analyses across a transect of the inactive chimney 3651-0938, exhibit relatively uniform concentrations of Sr, U, and Ba across the structure (Table 2b and Fig. 6b).

Concentrations of several trace elements are significantly higher in some of the inactive structures than in the active structures. This trend is most clearly defined by Mn concentrations, with up to 13.8 ppm (average

Fig. 4. Representative photomicrographs of nascent, mature, and old vent structures at Lost City. Photographs A, B, and C are in crossed-polarized light, D is in plane light. (a) Delicate, needle-like aragonite crystals form in the direction of fluid flow (towards the upper left corner of the photo). This image is from sample 3876-1436, an actively venting flange on the "Beehive" structure. (b) Sinuous, well-defined fluid flow paths (black) are preserved in carbonate (sample 3862-1659) filling a fissure. This deposit represents a mature system (Stage III), and is located on the side of the Poseidon edifice. (c) Relict, micritic calcite (mc)-filled fluid flow paths in the inactive structure 3867-1308. Brucite (brc) lines the channel walls. (d) Abundant fossils and shells of marine organisms are preserved in the outer walls of the inactive, old structure (sample 3651-0908).

Table 2a
Major element composition of Lost City carbonates

Sample ID	Type[c]	%Ca	%Mg	%Na	%K
3651-1022	A	20.34	13.37	0.64	0.05
3651-1149	A	21.56	12.20	0.94	0.04
3862-1219	A	21.03	13.82	0.50	0.03
3862-1325	A	25.23	8.91	0.88	0.04
3864-1524	A	27.98	4.12	1.49	0.07
3864-1537	A	14.24	18.40	1.16	0.07
3869-1443	A	15.85	18.38	0.45	0.05
3869-1446	A	10.60	25.60	0.86	0.07
3876-1436	A	28.11	3.50	0.74	0.00
3877-1606	A	12.71	21.27	1.84	0.07
3880-1532	A	12.00	20.53	1.85	0.11
3651-0908	I	31.36	2.43	0.38	0.07
3651-0938	I	33.39	0.25	0.45	0.01
3651-0938 0–1[a]	I	36.28	0.06	0.20	0.05
3651-0938 5–6[a]	I	36.03	0.00	0.12	0.02
3651-0938 9–10[a]	I	33.93	0.31	0.16	0.00
3651-0938 11–12[a]	I	33.42	0.45	0.17	0.02
3651-0938 12–13[a]	I	34.60	0.17	0.12	0.03
3651-1123	I	32.82	0.03	0.61	0.06
3651-1231	I	31.70	0.82	0.93	0.09
3862-1517bs	I	33.17	0.31	0.46	0.05
3862-1517tp	I	11.75	0.86	0.29	0.06
3863-1811	I	31.67	1.68	0.36	0.06
3864-1647	I	33.01	0.26	0.96	0.09
3867-1308	I	33.06	0.24	0.77	0.08
3871-1512	I	31.31	1.34	0.49	0.00
3872-1530	I	11.16	15.04	0.50	0.05
3873-1233	I	32.89	1.08	0.26	0.12
3876-1113	I	29.02	3.78	0.50	0.09
3881-1338/1[b]	I	23.88	11.52	0.83	0.05
3881-1338/2[b]	I	27.65	8.43	0.47	0.05
3881-1338/3[b]	I	26.92	8.73	0.38	0.03
3881-1338/4[b]	I	26.44	9.26	0.57	0.02
3881-1338/5[b]	I	22.74	12.46	0.70	0.06
3881-1338/6[b]	I	23.93	10.67	0.61	0.13
3881-1338/7[b]	I	25.43	9.05	0.55	0.04
3651-0944	F	5.27	27.70	0.75	0.08
3862-1659	F	24.07	10.85	0.65	0.08
3863-1551	F	20.90	14.27	0.43	0.04
3865-1322	F	22.36	10.54	0.64	0.02
3876-1219	F	28.86	3.21	0.67	0.04
3879-1258	F	31.27	2.02	0.82	0.05
3880-1353	F	32.52	0.72	0.50	0.00
3881-1132b	F	28.11	6.15	0.51	0.05

[a] Subsamples from basal transect of intact chimney 3651-0938 (see Section 2 for details).
[b] Subsamples from basal transect of intact chimney 3881-1338 (see Section 2 for details).
[c] Corresponds to carbonate type described in Table 1.

4.1 ppm) in the active structures to concentrations up to 216 ppm (average 42.1 ppm) in the inactive structures (Table 2b, Fig. 7a). In carbonate samples recovered from fissures, Mn concentrations vary from 0.88 ppm to 227 ppm (average 37.6 ppm), spanning the entire range observed in the active and inactive edifices. The inactive structures have concentrations of Sr that range from 326 ppm to 18952 ppm (average 9015 ppm) compared to their active counterparts that range from 3479 to 13601 ppm (average 6328 ppm Sr) (Table 2b and Fig. 7b). The carbonate fissure deposits have Sr concentrations that span values of 2184–12539 ppm, with an average of 6260 ppm.

The trace elements Ti, V, Cr, Ni, and Co increase from BDL values in the active structures, to concentrations ranging from 0.1 ppm to >40 ppm in the inactive structures (Table 2b). Concentrations of these trace elements vary with up to 61 ppm Ti, 16 ppm V, and 19.3 ppm Cr (Table 2b). Ni reaches concentrations up to 32 ppm, and Co ranges from <1 ppm in active structures up to 18 ppm in inactive structures (see Fig. 8 for average values). Ti concentrations are positively correlated with Mn concentrations in the inactive structures. Ni and Cr concentrations are higher in some of the fissure structures than in active or inactive deposits. Although the concentrations of these metals tend to increase with progressive aging of the structures, there is little co-variation in trace element concentrations.

4.4. Sr isotopes

A select set of Lost City vent fluids and carbonate structures was analyzed for $^{87}Sr/^{86}Sr$ ratios to examine the influence of seawater interactions during aging of the chimneys. Seven carbonate vent samples from active and inactive structures collected in 2000 were analyzed for Sr isotopes. Samples from three active structures that were analyzed include two from flanges and one piece from an actively venting fissure. The $^{87}Sr/^{86}Sr$ values in these samples range from 0.70757 to 0.70827, with an average ratio of 0.70794 (Table 2b). In contrast, the $^{87}Sr/^{86}Sr$ ratios from inactive structures range from 0.70862 to near-seawater values of 0.70913, with an average value of 0.70891 (Table 2b). Sr isotope ratios were measured in thirteen vent fluid samples, where temperatures ranged from 40 °C to 91 °C. Mg concentrations in these samples range from 0.91 mmol/kg to 35.44 mmol/kg (seawater Mg concentration = 52.9 mmol/kg) (Table 3). The $^{87}Sr/^{86}Sr$ ratios of vent fluids range from 0.70640 to 0.70802. Background seawater at 750 m was 0.70914 (Table 3).

5. Discussion

5.1. Hydrothermal flow at the LCHF

Several important factors facilitate hydrothermal flow at the LCHF: (1) within the vicinity of the field, a series of steeply dipping normal faults localize hydrothermal flow (Kelley et al., 2005; Karson et al., 2006); (2) seismic activity on the nearby east-west trending ATF (Smith et al., 2003) likely promotes and maintains permeability along established fault networks; (3) on the eastern side of the field in an area where seeps issue from near vertical cliffs, flow appears to be controlled by low angle, west-dipping faults associated with a 100 m thick shear zone (Kelley et al., 2005; Karson et al., 2006); and (4) additional fracturing of the basement rocks may be pro-

Table 2b
Trace metal and Sr isotope composition of Lost City carbonates

Sample ID	Type	Ti	V	Cr	Mn	Ni	Co	Cu	Sr	Mo	Ba	U	$^{87}Sr/^{86}Sr$[a]
% Accuracy		4.25	2.58	9.95	10.11	4.74	11.13	0.92	1.42	0.05	1.95	2.73	
% Precision		47.97	14.57	21.46	22.38	26.94	14.30	11.85	6.12	13.59	21.37	12.15	
Det. Limit (ppm rock)		73.32	3.37	23.27	24.92	16.11	0.82	1.98	4.20	5.69	19.86	23.97	
3651-1022	A	0.08	0.15	BDL	4.20	BDL	BDL	BDL	4788.67	0.11	15.73	2.30	0.70760
3651-1149	A	8.64	0.83	BDL	1.08	BDL	BDL	BDL	7255.62	0.33	25.40	3.73	0.70793
3862-1219	A	BDL	0.94	BDL	5.45	BDL	BDL	BDL	6615.44	0.60	22.67	3.42	
3862-1325	A	BDL	0.14	BDL	5.20	BDL	BDL	BDL	5698.39	0.09	21.77	2.36	
3864-1524	A	BDL	0.29	BDL	BDL	BDL	BDL	BDL	13601.48	0.10	23.91	5.06	
3864-1537	A	BDL	0.76	BDL	BDL	BDL	BDL	BDL	4977.53	0.38	19.61	2.96	
3869-1443	A	BDL	2.43	BDL	5.58	BDL	BDL	BDL	8200.50	1.68	22.52	5.80	
3869-1446	A	BDL	1.46	BDL	13.82	BDL	BDL	BDL	3481.44	1.53	10.55	3.49	
3876-1436	A	BDL	0.20	BDL	5.98	BDL	1.08	1.18	7364.21	BDL	23.17	2.94	
3877-1606	A	BDL	0.84	BDL	BDL	BDL	BDL	BDL	4151.23	0.32	17.03	2.32	
3880-1532	A	BDL	0.35	BDL	4.37	BDL	BDL	BDL	3478.82	0.12	17.89	2.63	
3651-0908	I	61.07	5.38	2.80	215.46	6.67	17.96	1.24	4215.61	0.03	13.09	0.73	0.70913
3651-0938	I	5.99	2.02	0.27	15.42	0.21	0.28	0.02	11487.34	0.02	28.07	9.90	0.70866
3651-0938 0-1[b]	I	9.22	1.37	2.49	16.36	0.71	0.47	BDL	14678.72	BDL	53.97	9.65	
3651-0938 5–6[b]	I	0.78	0.32	BDL	7.38	BDL	0.39	BDL	17126.79	BDL	24.36	8.65	
3651-0938 9–10[b]	I	2.43	0.39	0.21	17.32	0.41	0.62	BDL	16502.33	BDL	28.60	9.52	
3651-0938 11–12[b]	I	3.71	0.56	0.77	31.29	0.58	1.34	BDL	14724.62	BDL	23.03	9.16	
3651-0938 12–13[b]	I	9.41	2.26	0.94	73.38	2.07	2.02	BDL	16136.37	BDL	32.32	10.85	
3651-1123	I	BDL	0.42	BDL	6.04	0.19	0.09	BDL	18931.53	0.02	20.10	5.68	0.70908
3651-1231	I	1.98	0.90	0.04	4.83	0.13	BDL	BDL	15090.06	0.08	33.73	4.78	0.70896
3862-1517bs	I	3.47	0.25	BDL	15.89	BDL	BDL	BDL	12469.69	BDL	21.35	4.39	
3862-1517tp	I	0.16	0.25	BDL	9.57	BDL	BDL	BDL	4971.04	0.02	7.73	2.18	
3863-1811	I	60.81	2.92	BDL	135.43	4.33	6.86	0.13	4523.37	0.06	6.12	0.96	
3864-1647	I	12.29	1.44	1.27	47.27	0.87	2.31	0.07	18952.13	0.16	14.80	5.74	
3867-1308	I	40.73	2.44	8.05	97.38	4.50	4.19	0.07	17594.51	0.09	15.50	4.82	
3871-1512	I	15.98	6.21	0.63	55.49	4.99	2.97	0.22	15487.12	0.15	10.38	3.74	
3872-1530	I	2.26	16.89	0.65	145.19	4.84	BDL	0.38	5784.97	0.11	7.65	4.84	
3873-1233	I	57.25	2.81	2.64	139.70	11.31	7.72	0.24	1918.35	0.06	1.86	0.30	
3876-1113	I	BDL	1.24	BDL	5.84	BDL	BDL	BDL	4364.06	0.05	30.37	1.88	
3881-1338/1[c]	I	1.24	0.24	BDL	2.87	BDL	BDL	BDL	2221.89	0.05	16.70	2.13	
3881-1338/2[c]	I	BDL	0.01	BDL	4.25	BDL	BDL	BDL	326.10	BDL	0.14	0.97	
3881-1338/3[c]	I	0.29	BDL	BDL	3.31	BDL	BDL	BDL	345.86	BDL	0.70	0.99	
3881-1338/4[c]	I	BDL	0.02	BDL	1.35	BDL	BDL	BDL	931.32	BDL	6.50	1.49	
3881-1338/5[c]	I	BDL	0.25	BDL	1.26	BDL	BDL	BDL	1265.95	BDL	14.00	2.21	
3881-1338/6[c]	I	BDL	0.36	BDL	BDL	BDL	BDL	BDL	2545.88	0.04	26.74	2.00	
3881-1338/7[c]	I	BDL	0.28	BDL	BDL	0.02	BDL	BDL	2800.35	0.02	28.73	2.23	
3651-0944	F	5.29	1.31	BDL	3.68	BDL	BDL	0.72	2184.15	0.38	33.18	2.94	0.70799
3862-1659	F	0.01	0.91	BDL	1.62	BDL	BDL	BDL	8526.46	0.42	19.56	2.61	
3863-1551	F	BDL	1.53	BDL	0.88	BDL	BDL	BDL	7383.28	3.26	8.85	2.04	
3865-1322	F	0.24	1.76	BDL	3.33	BDL	BDL	BDL	6595.41	0.58	9.64	2.05	
3876-1219	F	0.12	1.70	2.68	227.33	BDL	BDL	BDL	4653.18	0.42	15.52	2.14	
3879-1258	F	9.85	4.93	19.31	21.23	31.95	1.02	BDL	5722.88	0.22	33.16	3.34	
3880-1353	F	5.48	1.23	1.56	28.42	1.29	0.65	BDL	12539.55	0.06	29.21	5.72	
3881-1132b	F	BDL	0.64	1.38	14.51	4.32	BDL	BDL	2481.98	0.28	11.92	2.00	

All concentrations are given in ppm. BDL signifies below detection limit.

[a] Sr isotope ratios normalized to $^{86}Sr/^{88}Sr = 0.1194$. All carbonate Sr isotope analyses completed at the UW and normalized to NBS 987 $^{87}Sr/^{86}Sr = 0.71024$.

[b] Subsamples from basal transect of intact chimney 3651-0938 (see Section 2 for details).

[c] Subsamples from basal transect of intact chimney 3881-1338 (see Section 2 for details).

moted by serpentinization, which can result in a volume increase of 20–40% (O'Hanley, 1996). It is likely that serpentinization-related expansion of the basement rocks promotes mass wasting on the free standing southern face of the massif. Together, these processes may lead to new and continuous exposure of fresh peridotite and deepening of preexisting fracture networks, allowing for continued fluid flow and precipitation of carbonate deposits.

5.2. Precipitation of $CaCO_3$ at Lost City

The geochemistry of the LCHF is dominantly controlled by the interaction of seawater with the underlying peridotite. The precipitation of calcium carbonate is driven by the pH of the vent fluids and the seawater carbonate buffer system. Carbonate acid–base chemistry and acidity constants dictate that high-pH fluids are dominated by bicarbonate and carbonate species. When these fluids come

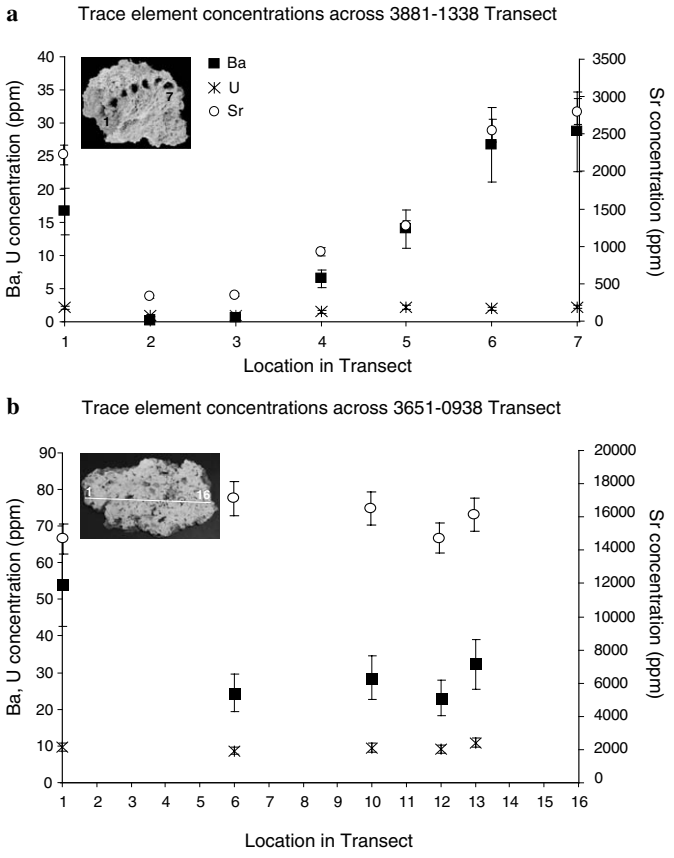

Fig. 6. (a) Ba, U, and Sr concentrations (ppm) in a basal transect of chimney 3881-1338, which is believed to have been recently active. The chimney is ~20 cm across and the distance between each sample location is ~2.5 cm. Trends in trace element composition are asymmetric. Ba and Sr increase linearly from points 2 to 7 in the structure, but there is a steeper compositional gradient between samples 1 and 2. U increases slightly from points 2 to 3 towards the exterior of the chimney (points 1 and 7). Error bars are % precision. The trends in trace metal composition suggest that the chemistry of the interior is controlled by vent fluids with low trace element concentrations. The increase in metals towards the exterior indicates the infiltration of seawater into the chimney. (b) Ba, U, and Sr concentrations (ppm) in subsamples from a basal transect of an older chimney, 3651-0938, that is most likely extinct. Symbols represent the same elements as in (a). The chimney is ~16 cm across and the distance between each sample location is ~1 cm. The concentrations of Ba, Sr, and U in this transect do not exhibit the same trends as those observed in sample 3881-1338, indicating that the chimney has been completely saturated by seawater.

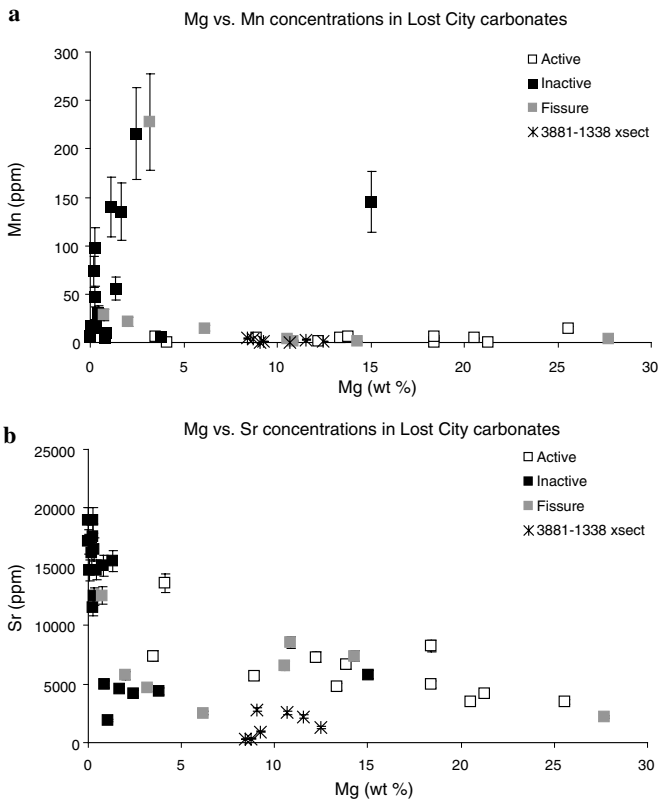

Fig. 7. (a) Mg vs. Mn (ppm) and (b) Mg vs. Sr (ppm) of Lost City carbonate samples. Samples are categorized as active, inactive, and fissure (see Section 3 for details). Samples from chimney 3881-1338 are collected from a basal transect, which may have been recently venting. In general, Mg concentrations of inactive structures are less than active structures. In some samples, Mn concentrations are higher in inactive structures than in those actively venting. Sr concentrations vary across all three sample types. Error bars are % precision. Increased Mn concentrations are likely due to the formation of Mn-oxides, while elevated Sr may be attributed to the formation of strontianite.

into contact with relatively acidic seawater, carbonate ions combine with Ca^{2+} ions from the vent fluid to form $CaCO_3$ (Palandri and Reed, 2004). Experimental studies show that aragonite is kinetically favored at temperatures >60 °C, while calcite is the dominant form of $CaCO_3$ at temperatures <15 °C (Kahmi, 1963; Vecht and Ireland, 2000). This is consistent with petrographic analyses of the Lost City samples, which show that aragonite is the first carbonate mineral to precipitate in the actively venting structures; followed by calcite in inactive structures that are bathed in seawater.

In addition to pH, the absence of Mg in endmember hydrothermal fluids at Lost City likely facilitates the precipitation and growth of the carbonate deposits [Mg^{2+} inhibits the nucleation of $CaCO_3$ (Pytkowicz, 1973; Bischoff et al., 1993a; Berndt and Seyfried, 1999)]. As seawater is entrained during mixing, brucite precipitates, removing Mg^{2+} from seawater and OH^- ions from the vent fluids (Allen and Seyfried, 2004; Palandri and Reed, 2004). Brucite is only stable in low-CO_2 fluids (Johannes and Metz, 1968; Moody, 1976). Progressive mixing with seawater causes the brucite to become unstable and dissolve. This process is the best explanation for the lack of brucite in older samples that have been continually exposed to seawater; this interpretation is also supported by theoretical models presented by Allen and Seyfried (2004) and Palandri and Reed (2004).

The Sr isotope composition of the chimneys (Table 2b), vent fluid, and seawater endmember compositions (Fig. 9) can be used to approximate the proportion of vent fluid and seawater that mixed to precipitate the carbonate. This fluid/seawater ratio can then be compared to mixing calculations presented by Allen and Seyfried (2004) and Palandri and Reed (2004) to deduce conditions of mineral precipitation. For example, sample 3651-1022 has a $^{87}Sr/^{86}Sr$ composition of 0.70760, which indicates that Sr in this sample

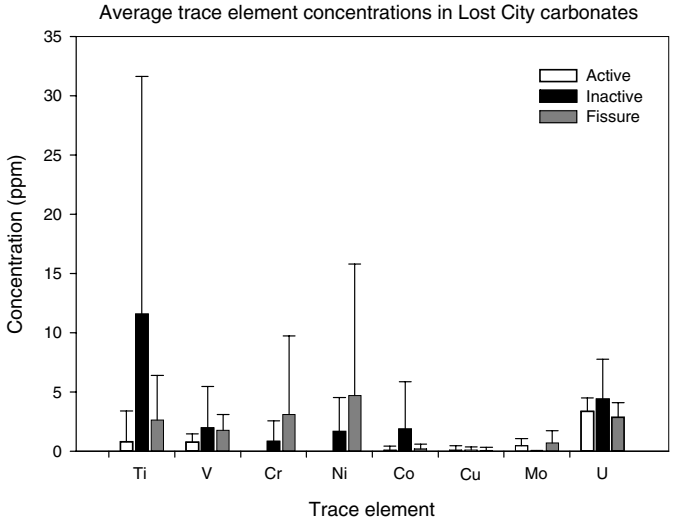

Fig. 8. Average concentrations of trace metals (Ti, V, Cr, Ni, Co, Cu, and Mo) in different types of Lost City carbonate structures. Error bars represent standard deviation. Although poorly correlated with structure type, in general trace element concentrations increase in older structures due to progressive infiltration by seawater.

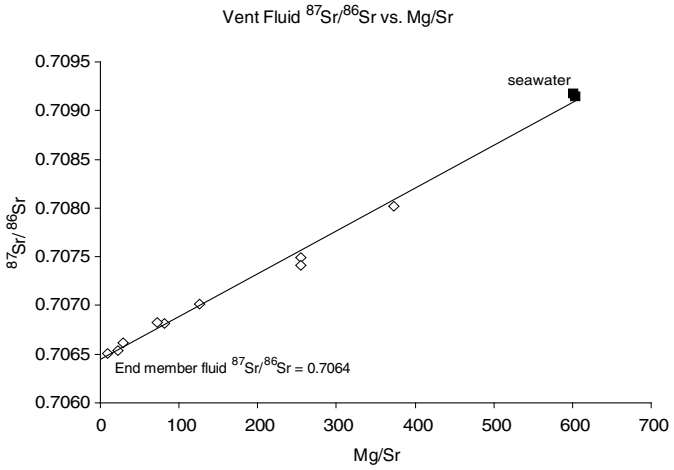

Fig. 9. Sr isotope vs. Mg/Sr ratios in Lost City vent fluids. Extrapolating the trend from seawater (SW) composition to zero magnesium, the $^{87}Sr/^{86}Sr$ of an endmember fluid at Lost City is 0.7064. This value is likely representative of the Sr isotope composition of deep-seated fluids.

precipitated from a mixture of ~60% vent fluid and ~40% seawater. Using Sr as a proxy for carbonate precipitation and comparing this to Palandri and Reed's model (2004), this rock should be a mix of calcium carbonate and slightly less brucite. Accordingly, this sample contains 20.34 wt% Ca and 13.37 wt% Mg. In contrast, sample 3651-0908 has a Sr isotope ratio of 0.70913, indicating that it is mostly (near 100%) seawater-derived carbonate. According to geochemical models in Palandri and Reed (2004), this sample should be composed of only calcium carbonate. This sample contains 31.36 wt% Ca and 2.43 wt% Mg; thus, geochemical analyses of the Lost City carbonates match relatively well with results of predictive models presented in earlier studies.

5.3. Aging and evolution of carbonate structures over time

5.3.1. Evolution of mineralogy and porosity

Sinuous, fine channels interpreted to be fluid flow conduits, facilitate diffuse flow within actively venting structures at Lost City (Fig. 4b). Some of these microconduits may result from nucleation of carbonate minerals on cm-long strands of filamentous bacteria that commonly colonize the exterior of active structures (Kelley et al., 2005). As the edifices age and become increasingly infiltrated by seawater, these channels progressively fill with calcite, which is saturated in the North Atlantic at depths of <4500 m (Pilson, 1998). Micritic calcite is common in older chimneys, where it typically fills former flow channels (Fig. 4c). This infilling process decreases porosity and increases the lithification and strength of the structures. Many of the oldest deposits have the appearance of massive, natural concrete, and show little evidence of past fluid conduits within their walls (Fig. 4d).

Within young to moderately old chimneys, brucite forms within the walls during mixing of endmember high-pH, high (OH^-)-bearing vent fluids, and Mg-rich seawater. Brucite is less abundant than the carbonate minerals, and it is most common in young, active chimneys where it lines channel walls (Fig. 4c). However, brucite is ephemeral within the chimneys because it becomes unstable in cooler

Table 3
Mg concentrations and Sr isotope ratios of Lost City vent fluids

Sample ID[a]	Site	Depth (m)	Temp (°C)	pH	Mg (mmol/kg)	Sr (mmol/kg)	Mg/Sr	$^{87}Sr/^{86}Sr$[b]
3862m11	Poseidon, S side	730	59	10.20	8.13	0.1006	80.81	0.70682
3863m11	Poseidon	731	81	10.67	3.02	0.1051	28.76	0.70662
3864m23	Imax Flange	764	62	10.97	2.32	0.1040	22.27	0.70654
3866p23	Marker 7	801	47	8.70	35.44	0.0950	372.97	0.70802
3866b16	Near Marker 7	801	51	9.33	24.90	0.0975	255.24	0.70749
3870bf17	Marker 8	802	51	9.96	7.05	0.0980	71.96	0.70683
3874b9	Marker C	780	73	10.06	12.02	0.0957	125.66	0.70701
3874b18	Beehive	743	91	10.71	0.91	0.0948	9.56	0.70651
3880m24	Marker H	845	30	9.76	24.09	0.0945	254.89	0.70741
3870b19	Background seawater	789	10	7.98	53.12	0.0880	603.33	0.70914
3882m23	Background seawater	~3680	~7	~8	54.29	0.0903	601.50	0.70917

[a] Fluid samples were collected using a variety of sampling devices: m, titanium major bottles; b or p, HFPS; bf, filtered HFPS samples.
[b] Sr isotope ratios measured at ETHZ. All ratios are normalized to $^{86}Sr/^{88}Sr = 0.1194$ and NBS 987 $^{87}Sr/^{86}Sr = 0.71024$.

fluids that contain less than ~35% vent fluid (Allen and Seyfried, 2004; Palandri and Reed, 2004). This leads to its dissolution during aging of the structures as venting ceases and the porous interior walls become saturated with seawater. This interpretation is supported by both XRD and major element data, which show that the active chimneys are composed of varying proportions of aragonite, calcite, and brucite, with near equal amounts of Ca and Mg. In contrast, the inactive structures show increasing amounts of calcite and minor brucite, which is also reflected in changes in bulk compositions to values of >30 wt% Ca and <5 wt% Mg (Tables 1, 2a, and 2b).

Aragonite within this system is metastable, converting to calcite over time. Berndt and Seyfried (1999) demonstrated that aragonite converts to calcite at a relatively slow rate of 10 μm/yr at 25 °C, but increases to 100 μm/yr at 100 °C. This conversion rate is dependent on both temperature and on the surface area of existing aragonite. The young structures at Lost City are dominated by aragonite and brucite, and are awash in ~40 °C to 91 °C vent fluids. Within the chimneys, the conversion of aragonite to calcite is most likely continuous at these temperatures, but slows during the later stages of chimney development, where cooler temperatures and exposure of extensive surface areas of aragonite promote dissolution.

5.3.2. Geochemical changes: trace elements

No clear trend is observed when comparing the concentrations of Na and K to other trace elements. To a first order, Na and K concentrations can be used to estimate the amount of seawater dried in the structures (samples were not rinsed in DIW after collection). The amount of sodium in the chimneys ranges from ~0.5 wt% to 1.5 wt%. However, because there is no relationship between Na, K, and trace element concentrations in the chimneys, we assume that the measured trace element concentrations are not an artifact of dried seawater.

The elevated concentrations of Mn in some of the inactive structures (Fig. 7a) can be attributed to uptake of Mn during calcite precipitation (Veizer, 1983; Rimstidt et al., 1998) and to the formation of Mn-oxide on the exterior of the inactive structures. The older, inactive edifices exhibit a dark exterior that is likely due to the formation of Mn-oxides (Fig. 3). Mn-coatings are also common on the exterior of metagabbroic and serpentinite samples recovered from the walls of the massif.

The relatively low temperature and high pH of the Lost City fluids are responsible for the lack of metals in both the endmember vent fluids and the active structures. Progressive bathing of inactive structures in seawater results in the incorporation of the trace elements Co, Cr, V, and Ni into the carbonate structures. Ti likely co-precipitates with Mn-oxides that form on the exterior of the structures over time (as indicated by the positive correlation between Mn and Ti). The elevated concentrations of Ni and Cr in some of the serpentinite fissure deposits is attributed to localized uptake from the enclosing serpentinite basement rock, which has high concentrations of Ni and Cr (Boschi et al., 2006).

As described in Section 4.3, some inactive chimneys have elevated Sr concentrations (average 9015 ppm) compared to active chimneys [average 6328 ppm Sr (Table 2b and Fig. 7b)]. This relationship is contrary to predictions based solely on the distribution coefficients of Sr in aragonite and calcite. The distribution coefficient for Sr in aragonite is 0.9–1.2, whereas in calcite it is 0.027–0.4 (Veizer, 1983). This implies that Sr should be higher in the aragonite-dominated, active structures. Lost City samples show an inverse of this trend (Fig. 7b), which cannot be explained by the phase change from aragonite to calcite. The most likely explanation for the increase in Sr in the inactive chimneys is the formation of another phase. We hypothesize that trace strontianite may account for the increased concentrations of Sr in the inactive structures. It is also possible that distribution coefficients that are based on lacustrine and coralline environments may not apply to the warm, high-pH, reducing environment at Lost City.

Endmember LCHF vent fluids have near-zero concentrations of U (<0.2 ppb) and have elevated concentrations of Ba (~180 ppb) compared to average seawater concentrations (3 ppb U and 13.7 ppb Ba) (Pilson, 1998). The concentrations of Ba and U are variable in bulk rock analyses of active, inactive, and fissure structures. However, the basal transect across sample 3881-1338 illustrates a direct correlation between Ba, U, and Sr concentrations at a centimeter-scale (Fig. 6a) and support field observations that this pinnacle may have been recently active. The walls (points 1, 6, and 7) are elevated in Ba and Sr, while these elements are much lower in concentration in the interior of the chimney (points 2, 3, and 4). Although asymmetric, the low concentrations of trace elements such as U and Sr indicate that the interior of this chimney (near points 2 and 3) was a vent fluid-dominated environment, insulated from surrounding seawater. In contrast, samples closer to the exterior (points 1, 4, 6, and 7) show evidence for seawater entrainment into the structure, resulting in higher concentrations of U and Ba. Barium likely increases in the exterior of this chimney due to the precipitation of trace barite, which is saturated in seawater (as more seawater becomes entrained in the walls of the chimney, barite precipitates). The elevated concentrations of Sr towards the exterior may be due to the formation of trace strontianite with vent fluid-seawater mixing. By comparison, this trend does not appear to be preserved in older samples. Several subsamples collected along a basal transect of the old, extinct chimney 3651-0938 show relatively uniform concentrations of Sr and Ba (Fig. 6b). The rock chemistry has been significantly altered by seawater infiltration, recrystallization, and diagenesis.

5.3.3. Geochemical changes: Sr isotope ratios

The $^{87}Sr/^{86}Sr$ ratio of vent fluids and hydrothermal deposits is a measure of Sr leached from basement rocks and mixing of Sr from surrounding seawater (e.g., Teagle et al., 1998). Mid-Atlantic Ridge basalt samples from the MARK area have an average $^{87}Sr/^{86}Sr$ ratio of 0.7022 (Palmer, 1992). $^{87}Sr/^{86}Sr$ ratios of black smoker vent fluids reflect mixing between seawater ($^{87}Sr/^{86}Sr = 0.70918$) and host rock strontium (Palmer, 1992; Teagle et al., 1998; Butterfield et al., 2001). Analyses of fluids from the MARK and TAG sites on the MAR show that these fluids typically contain a large component of basaltic-derived Sr, with $^{87}Sr/^{86}Sr$ ratios ranging from an average of 0.7028 to 0.7029, respectively (Palmer and Edmond, 1989; Palmer, 1992; Teagle et al., 1998).

Within black smoker systems, Mg is removed from seawater via water-rock interactions producing fluids with a zero-Mg endmember (e.g., Butterfield et al., 1994; Mottl and Wheat, 1994; Von Damm, 1995; Wheat and Mottl, 2000). This has been well documented at volcanically-driven, basalt-hosted black smoker sites along the mid-ocean ridge network (Von Damm, 1995; Butterfield et al., 1997; Von Damm, 2000) and ultramafic-hosted black smoker systems such as the Rainbow and Logatchev fields on the MAR (Charlou et al., 2002). The hottest vent fluid samples at the LCHF yield Mg concentrations of <1 mmol/kg, indicating that a zero-Mg endmember fluid is also produced during serpentinization reactions (Kelley et al., 2005). Analyses of LCHF fluids show that there is a near-linear mixing trend between seawater and vent fluid (Kelley et al., 2001): this relationship was used to estimate an endmember composition for the $^{87}Sr/^{86}Sr$ ratio of vent fluid at the LCHF. Extrapolating the vent fluid $^{87}Sr/^{86}Sr$ ratios against Mg/Sr to a zero-Mg, endmember fluid, yields a $^{87}Sr/^{86}Sr$ value of 0.7064 (Fig. 9). This value is likely representative of deep-seated fluids flowing through the stockwork system within the massif and reflects the less radiogenic Sr isotopic composition of the basement rock.

Sr isotope ratios of the inactive structures are much higher than the values in the vent fluids and active chimneys because of their prolonged exposure to seawater and the subsequent incorporation of more radiogenic seawater Sr into the carbonate. In some cases (e.g., sample 3651-0938), the higher isotope ratios also correspond to increased concentrations of Sr in the inactive structures, reflecting the transformation from a vent fluid- to a seawater-dominated environment.

5.4. Growth model for Lost City carbonate structures

Analyses of a diverse suite of carbonate samples from the LCHF define five stages of development in the formation and evolution of the carbonate chimneys (Fig. 10). Carbonate veins hosted by serpentinite basement rock represent the paleo-plumbing system for the vent field. In some places, these veins are exposed on the surface, but similar fractures must lace the interior of the massif. The vein networks mark the beginning of carbonate precipitation and the first stage in development of the carbonate structures (Figs. 2a and 10). In this model, fluids travel via networks of fractures and cracks within the massif and ultimately reach the outer surface of the serpentinite basement rock. Here, diffusely venting hydrothermal fluids egress and aragonite and brucite minerals precipitate, filling the cracks, and fissures in the bedrock. Examples of structures in this first stage of growth include samples 3862-1659 and 3863-1551 (Tables 1, 2b, and Figs. 2a, 4b).

With continued venting and isolation of subsurface conduits via mineral precipitation, the structure grows upward and outward. Existing aragonite and calcite crystals provide nucleation sites for the precipitation of additional calcium carbonate and the structures increase in size. This second stage of development is characterized by extremely delicate, porous, friable edifices with fluid flow paths that are defined by the direction of crystal growth (Fig. 4a). These deposits are young in age (modern to 500 years) (Früh-Green et al., 2003) and are dominated by aragonite and brucite. Many of these structures exhibit flange and beehive morphologies and vent the hottest fluids (91 °C). These fluids also have the lowest measured Mg concentrations (<1 mmol/kg) and lowest $^{87}Sr/^{86}Sr$ ratios (0.70642) (Table 3). The low trace element contents of these young structures reflect the fact that mineral precipitation is dominated by the composition of primary endmember fluids that are low in most trace elements. Carbonate minerals in these structures have Sr isotope ratios close to those of the fluids (Table 2b). Examples of structures in this stage of development are 3651-1022, 3862-1524, 3876-1436, and 3880-1532 (Tables 1, 2b, and Figs. 2b, c, 4a).

In the third stage of development, calcite continues to be incorporated into the structure by conversion of aragonite to calcite and continued precipitation of calcite from surrounding seawater mixing with vent fluids. Brucite lines the fluid channels (Fig. 4c). Although flow paths during this growth stage are well-defined, they do not trend in any consistent direction. Instead, they are sinuous and meandering (Fig. 4b), leading to widespread, diffuse emanation of hydrothermal fluids. Structures in this third stage of development have slightly higher trace element concentrations, and higher $^{87}Sr/^{86}Sr$ ratios, reflecting continued mixing with seawater. Samples 3651-0944, 3862-1325, 3869-1443, and 3881-1338 are examples of structures in this stage of development (Tables 1, 2b, and Figs. 2c, 4b).

As venting wanes, the structures are increasingly saturated with seawater. This change in fluid chemistry and temperature defines the fourth stage of evolution. Fluid flow channels begin to fill with recrystallized calcite, leading to lithification, and strengthening of the structures. Porosity decreases to $<\sim$30%. Aragonite progressively converts to calcite and brucite becomes unstable and dissolves into surrounding seawater, leading to lower Mg contents of these samples. Some of the structures incorporate

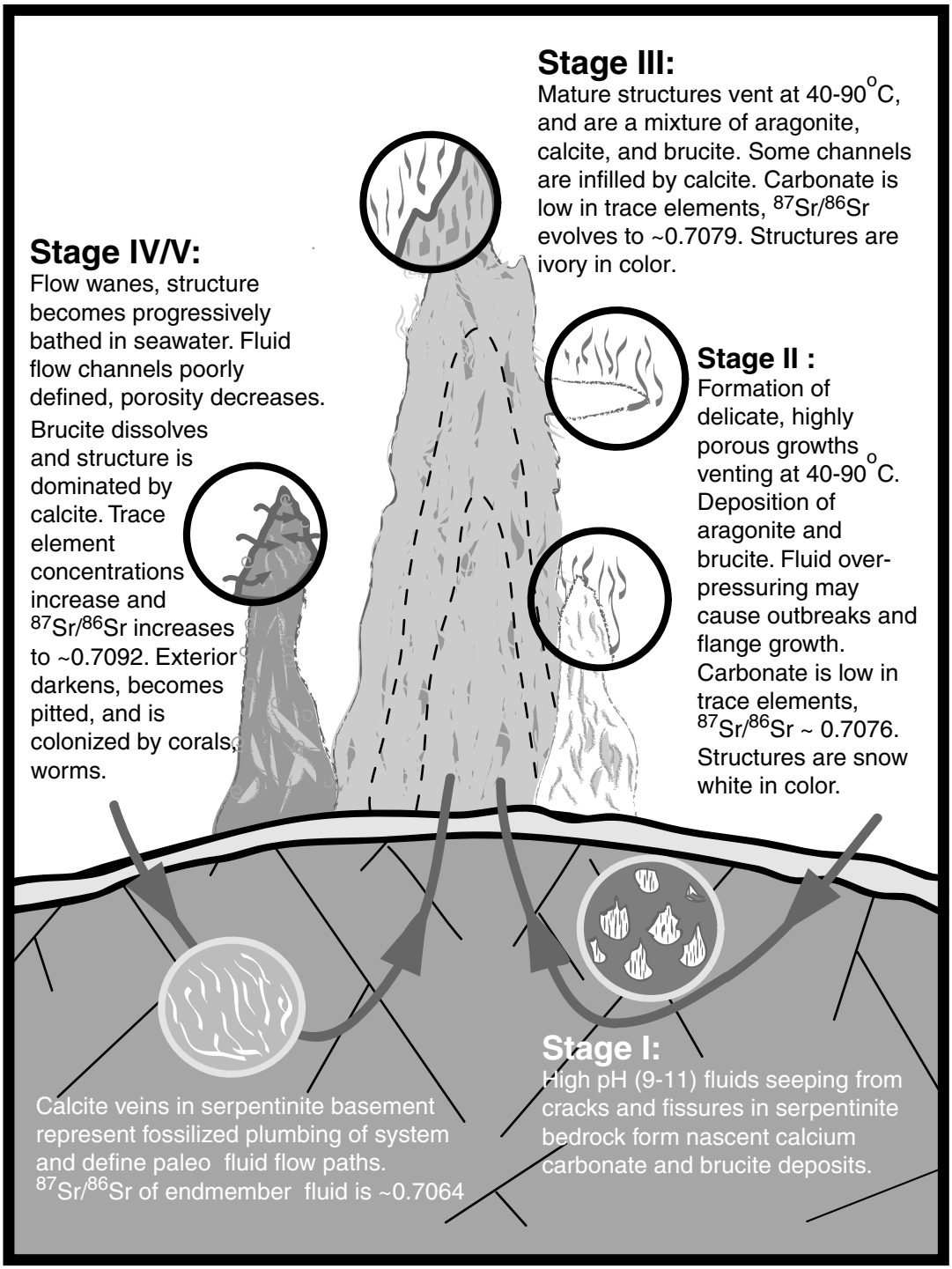

Fig. 10. Growth model schematic for carbonate deposits at the Lost City Hydrothermal Field. Five stages of development are defined by petrographic and geochemical differences. See text for details.

higher concentrations of trace elements and the carbonates have higher $^{87}Sr/^{86}Sr$ ratios due to diagenetic processes and continued seawater infiltration (Table 2b). The exteriors of the deposits darken in color due to manganese oxide precipitation associated with aging. Over time, coral polyps begin to colonize the outside of these older, cooler structures. The chimney walls incorporate fossils of marine organisms, serpulid worms, and gastropods. Examples of structures in this stage of development are 3651-1123, 3862-1517, and 3864-1647 (Tables 1, 2b, and Figs. 3a, 4c).

Extinct deposits that are up to 30,000 years old (Früh-Green et al., 2003) represent the final evolutionary stage for Lost City chimneys. These edifices have been extensively bathed in seawater and are dominated by calcite. Some samples have very localized "pockets" of aragonite and brucite, which may represent relatively young areas of

growth that have been isolated from seawater infiltration. These structures are generally dense and massive, and flow channels are no longer discernable (Fig. 5d). The walls of these deposits are dark brown and knobby and contain abundant fossils of marine organisms (Fig. 3c). Corals, worms, gastropods, and other small organisms are common on the outside of these structures (Kelley et al., 2005). Because of their prolonged exposure to seawater and the formation of Mn-oxides, some of these deposits contain high concentrations of trace elements such as Ti, Mn, and Sr, and Sr isotope ratios are near that of seawater (Table 2b). Examples of structures in this final stage of development are 3651-0908, 3651-0938, 3651-1231, and 3871-1512 (Tables 1, 2b, and Figs. 3b, c, and 4d).

5.5. Comparison of Lost City to other environments

Hydrothermal calcium carbonate precipitates are found in many environments. There are several well-studied, modern and ancient, marine, and terrestrial locations that are geochemically and structurally comparable to some of the characteristic features of the LCHF described above (Table 4).

Carbonate-veined serpentinites and carbonate-serpentine breccias (ophicalcites) are common in ophiolite complexes in the Alps (Lemoine, 1980; Weissert and Bernoulli, 1985; Bernoulli and Weissert, 1985; Früh-Green et al., 1990) and in the northern Apennine Mountains in Italy (e.g., Cortesogno et al., 1981; Treves and Harper, 1994; Treves et al., 1995). Ophicalcites are believed to have formed during hydrothermal and tectonic processes associated with serpentinization in fracture zone environments, or during exhumation of subcontinental mantle along passive margins (Desmurs et al., 2001; Bernoulli et al., 2003). In these environments, carbonate veins may represent paleo-stockwork systems similar to those beneath the LCHF (Kelley et al., 2005). Oxygen isotopes of carbonate material in ophicalcite veins indicate paleo fluid temperatures of $<150\,^{\circ}C$ (Barbieri et al., 1979; Weissert and Bernoulli, 1984; Früh-Green et al., 1990; Treves and Harper, 1994) similar to those at Lost City (Früh-Green et al., 2003).

Calcified serpentinites and serpentinite breccia deposits recovered from ODP Sites 897, 899, and 1068 in the ocean-continent transition zone in the Iberian Margin are comparable to ophicalcites and may be similar to rocks underlying the LCHF (Milliken and Morgan, 1996; Morgan and Milliken, 1996; Alt and Shanks, 1998; Beard and Hopkinson, 2000; Hopkinson et al., 2004). Veins within serpentinites and serpentinite breccias from Sites 897, 899, and 1068 are composed predominantly of calcium carbonate (Milliken and Morgan, 1996) and the precipitation of these carbonate minerals is attributed to the mixing of Ca-rich fluids from serpentinization reactions with seawater (Milliken and Morgan, 1996; Morgan and Milliken, 1996; Beard and Hopkinson, 2000; Hopkinson et al., 2004).

Morphologically, the carbonate chimneys at the LCHF resemble the unusual formations in Ikka Fjord, Greenland (e.g., Pauly, 1963; Buchardt et al., 1997; Buchardt et al., 2001) and the thinolite tufa structures in areas such as Mono Lake, California (e.g., Shearman et al., 1989; Bischoff et al., 1993a,b). Similar to Lost City chemistry, the tufa towers in both the Ikka Fjord and on the shores of Mono Lake result from mixing warm, high pH ($\sim$10), calcium-rich spring waters with cool, bicarbonate, and carbonate-rich lake water (Bischoff et al., 1993b; Buchardt et al., 1997) (Table 4).

Fluids issuing from serpentine mud volcanoes, such as those found in the Mariana forearc, reveal a different fluid chemistry than those at the LCHF even though fluids in both environments are influenced by serpentinization reactions (Fryer et al., 1990; Fryer, 1996; Fryer et al., 1999; Kelley et al., 2001; Mottl et al., 2003, 2004; Kelley et al., 2005). Fluids emanating from Marianas mud volcanoes in part originate from dehydration of the subducting slab (Fryer et al., 1990; Mottl, 1992; Fryer, 1996; Fryer et al., 1999; Mottl et al., 2003). The extremely high pH fluids (9.3–12.5) egress from seeps at $\sim$2 °C and vent diffusely through surrounding serpentine mud (Fryer et al., 1990; Mottl et al., 2004) (Table 4). Mixing of seawater with alkaline fluids from the serpentine mud volcanoes results in the precipitation of brucite and/or aragonite (Haggerty, 1987; Fryer et al., 1990, 1999; Haggerty, 1991; Mottl et al., 2004).

These examples show that processes similar to those at the LCHF have been operative in the past and continue to play an important role in creating high pH hydrothermal environments that remain poorly understood. Although we are gaining new insights into these novel high pH environments, there is much yet to learn about the fine-scale geochemistry of these systems, the life they support, and how these terrestrial and marine analogs compare to our observations at the LCHF.

6. Summary and conclusions

This study provides the first detailed mineralogical and chemical analyses of carbonate chimneys within the serpentinite-hosted LCHF. Our results show that the massive edifices form through complex fluid-chemical-mineralogical reactions over tens of thousands of years. Petrographic and geochemical analyses of a representative suite of samples define five stages of formation. These stages include the transformation from nascent, fragile, and highly porous active chimneys that are dominated by aragonite and brucite, to highly lithified, inactive deposits dominated by calcite and extinct deposits that lack well-defined flow channels. In these later stages, brucite dissolves resulting in decreased concentrations of Mg. Concomitant with mineralogical and physical changes during aging, the chimneys tend to become enriched in seawater-derived trace metals and Sr isotope ratios increase toward seawater values.

Table 4
Comparison of hydrothermal deposits

Location	Ikka Fjord, Greenland	Mono Lake, California	Conical Seamount Marianas	Lost City, MAR	Rainbow, MAR
Tectonic Environment	Continental fjord	Volcanic caldera	Subduction zone	Oceanic core complex	Spreading center
Type of Venting	Cold seeps	Hydrothermal springs	Diffuse seeps, chimneys	Hydrothermal chimneys	Hydrothermal chimneys
Basement Rock	Syenite, carbonitite	Rhyolite	Serpentinized mud	Serpentinized peridotite, gabbro	Serpentinized peridotite, gabbroic intrusions?
Precipitate Type	Tufa towers, 1–20m tall	Tufa towers, 1–3m tall	Carbonate towers up to 1.5m tall	Carbonate towers, 30–60m tall	Sulfide chimneys
Precipitate Mineralogy[a]	cc, ik, hmc	arag, cc, ik, gay	arag, brc, calcite, ams	arag, cc, brc, ik?	Sulfide minerals
$^{87}Sr/^{86}Sr$ Fluid	0.70855–0.70918		<0.7062	~0.7064	
$^{87}Sr/^{86}Sr$ Precipitate	0.70916			0.7076–0.7091	
Source Water	Meteoric	Meteoric	Dehydrated slab fluid	Seawater	Seawater
Source Water					
Temp (°C)	1.3	3–6	1.67	~7	~7
pH	8.1	9.7–10.0	8.1	7.9	7.8
[Ca] (mmol/L)	8.9	4	10.3	10.4	10.2
[Mg] (mmol/L)	45.7	33	52.3	54.4	53
alk (meq/kg)	<0.5	36201[c]	2.59	2.51	—
Fluid					
Temp (°C)	3.1–4.1	8–18, 35[b]	1.5 (from chimney)	40–91	365
pH	10.4	6.4–6.8	9.3–12.5	9–10.8	3.3
[Ca] (mmol/L)	0.17	111–169	0.6–1	21.0–23.3	67
[Mg] (mmol/L)	1.7	23–83	0.003–0.009	<1	0
alk (meq/kg)	153	566-1891[c]	41–52	1.2–4.7	
References	[d,e]	[f,g]	[h,i,j,k]	[l,m,n]	[o,p]

[a] Mineral abbreviations: arag, aragonite; cc, calcite; brc, brucite; ik, ikaite; hmc, high-Mg calcite; gay, gaylussite; ams, amorphous-Mg silicate.
[b] Measured from top of tufa tower.
[c] Alkalinity as mg/L HCO_3.
[d] Marland (1975).
[e] Buchardt et al. (1997).
[f] Bischoff et al. (1993b).
[g] Council and Bennett (1993).
[h] Fryer et al. (1990).
[i] Fryer (1996).
[j] Fryer et al. (1999).
[k] Mottl et al. (2004).
[l] Kelley et al. (2001).
[m] Früh-Green et al. (2003).
[n] Kelley et al. (2005).
[o] Charlou et al. (2002).
[p] Douville et al. (2002).

The chemical composition of carbonate deposits and vent fluids within the Lost City field and its extended history of venting are likely the product of extensive faulting within the Atlantis Massif and long-lived serpentinization reactions in the subsurface. Complex networks of carbonate veins and fissure-filling deposits within the serpentinized basement rocks correspond to the progressive funneling of hydrothermal fluids from depth to the surface. These veins are reminiscent of ophicalcite deposits in ancient ophiolite deposits.

The Lost City hydrothermal system represents a novel, natural laboratory for investigating linkages between geological, biological, and hydrothermal processes in a system dominated by moderate temperature serpentinization reactions. Although the LCHF is the first of its kind to be investigated, future studies will likely show that it is not unique to mid-ocean ridge environments and that similar systems have probably been operating throughout much of Earth's history. We do not yet know the impact that Lost City-like systems have on global geochemical budgets, but this will be an important avenue of study in follow-on investigations of off-axis serpentinite-hosted environments.

Acknowledgments

We thank S. Emerson for use of his analytical facility at the UW and C. Stump for technical assistance with the ICP-MS; M. Frank at ETHZ for fluid Sr isotope analyses; J. Karson for helpful discussions on the geology of the massif; M. Elend for assistance with image archiving and processing; and P. Fryer for supportive information on the Marianas mud volcanoes. We greatly appreciate the help and support of the Alvin-Atlantis crew and our colleagues during the AT07-34 cruise. We thank associate editor J. Alt for thoughtful guidance and insights on this publication. We appreciate M.J. Mottl and two anonymous reviewers who provided detailed comments and suggestions that contributed significantly to the improvement of this manuscript. This work was funded by NSF Grant OCE0137206 to D.S. Kelley and Swiss SNF Grant 2100-068055 to Früh-Green.

Associate editor: Jeffrey C. Alt

References

Allen, D.E., Seyfried, W.E., 2004. Serpentinization and heat generation: constraints from Lost City and Rainbow hydrothermal systems. *Geochim. Cosmochim. Acta* **68**, 1347–1354.

Alt, J.C., Shanks, W.C., 1998. Sulfur in serpentinized oceanic peridotites: serpentinization processes and microbial sulfate reduction. *J. Geophys. Res.* **103**, 9917–9929.

Bach, W., Banerjee, N.R., Dick, H.J.B., Baker, E.T., 2002. Discovery of ancient and active hydrothermal systems along the ultra-slow spreading Southwest Indian Ridge 10–16°E. *Geochem. Geophys. Geosys.* **3** (7). doi:10.1029/2001GC000279.

Baker, E.T., Edmonds, H.N., Michael, P.J., Bach, W., Dick, H.J.B., Snow, J.E., Walker, S.L., Banerjee, N.R., Langmuir, C.H., 2004. Hydrothermal venting in magma deserts: the ultraslow spreading Gakkel and Southwest Indian Ridges. *Geochem. Geophys. Geosys.* **5** (8). doi:10.1029/2004GC000712.

Barbieri, M., Masi, U., Tolomeo, L., 1979. Stable isotope evidence for a marine origin of ophicalcites from the north-central Apennines (Italy). *Mar. Geol.* **30**, 193–204.

Batuyev, B.N., Krotov, A.G., Markov, V.F., Cherkashev, G.A., Krasnov, S.G., Lisitsyn, Y.D., 1994. Massive sulfide deposits discovered and sampled at 14°45′N, Mid-Atlantic Ridge. *BRIDGE Newslett.* **6**, 6–10.

Beard, J.S., Hopkinson, L., 2000. A fossil, serpentinization-related hydrothermal vent, Ocean Drilling Program Leg 173, Site 1068 (Iberia Abyssal Plain): some aspects of mineral and fluid chemistry. *J. Geophys. Res.* **105**, 16527–16539.

Berndt, M.E., Seyfried, W.E., 1999. Rates of aragonite conversion to calcite in dilute aqueous fluids at 50 to 100 °C: experimental calibration using Ca-isotope attenuation. *Geochim. Cosmochim. Acta* **63**, 373–381.

Bernoulli, D., Manatschal, G., Desmurs, L., Muntener, O., 2003. Where did Gustav Steinmann see the trinity? Back to the roots of an Alpine ophiolite concept. In: Dilek, Y., Newcomb S. (Eds.), *Ophiolite Concept and the Evolution of Geological Thought* Boulder, Geological Society of America Special Paper **373**, 93–110.

Bernoulli, D., Weissert, H., 1985. Sedimentary fabrics in alpine ophicalcites, South-Pennine Arosa zone, Switzerland. *Geology* **13**, 755–758.

Bischoff, J.L., Fitzpatrick, J.A., Rosenbauer, R.J., 1993a. The solubility and stabilization of ikaite ($CaCO_3{\cdot}6H_2O$) from 0 to 25 °C: environmental and paleoclimatic implications for thinolite tufa. *J. Geol.* **101**, 21–33.

Bischoff, J.L., Stine, S., Rosenbauer, R.J., Fitzpatrick, J.A., Stafford, T.W., 1993b. Ikaite precipitation by mixing of shoreline springs and lake water, Mono Lake, California, USA. *Geochim. Cosmochim. Acta* **57**, 3855–3865.

Blackman, D.K., Cann, J.R., Janssen, B., Smith, D.K., 1998. Origin of extensional core complexes: evidence from the Mid-Atlantic Ridge at Atlantis Fracture Zone. *J. Geophys. Res.* **103**, 21315–21333.

Blackman, D.K., Karson, J.A., Kelley, D.S., Cann, J.R., Früh-Green, G.L., Gee, J.S., Hurst, S.D., John, B.E., Morgan, J., Nooner, S.L., Ross, D.K., Schroeder, T.J., Williams, E.A., 2002. Geology of the Atlantis Massif (Mid-Atlantic Ridge, 30°N): implications for the evolution of an ultramafic oceanic core complex. *Mar. Geophys. Res. Lett.* **23**, 443–469.

Bogdanov, Y., Sagalevitch, A., Chernayev, E., Ashadze, A., Gurvich, E., Lukaskin, V., Ivanov, G., Peresypkin, V., 1995. A study of the hydrothermal field at 14°45′ on the Mid-Atlantic Ridge using the MIR submersibles. *BRIDGE Newslett.* **9**, 9–13.

Boschi, C., Früh-Green, G.L., Delacour, A., Karson, J.A., Kelley, D.S., 2006. Mass transfer and fluid flow during detachment faulting and development of an oceanic core complex, Atlantis Massif (MAR 30 °N). *Geochem. Geophys. Geosyst.* **7**. doi:10.1029/2005GC001074.

Buchardt, B., Seaman, P., Stockmann, G., Vous Uffe Wilken, M., Duwel, L., Kristiansen, A., Jenner, C., Whiticar, M.J., Kristensen, R.M., Petersen, G.H., Thorbjorn, L., 1997. Submarine columns of ikaite tufa. *Nature* **390**, 129–130.

Buchardt, B., Israelson, C., Seaman, P., Stockmann, G., 2001. Ikaite tufa towers in Ikka Fjord, southwest Greenland: their formation by mixing of seawater and alkaline spring water. *J. Sediment. Res.* **71**, 176–189.

Butterfield, D.A., McDuff, R.E., Mottl, M.J., Lilley, M.D., Lupton, J.E., Massoth, G.J., 1994. Gradients in the composition of hydrothermal fluids from the Endeavor Segment vent field; phase separation and brine loss. *J. Geophys. Res.* **99**, 9561–9583.

Butterfield, D.A., Jonasson, I.R., Massoth, G.J., Feely, R.A., Roe, K.K., Embley, R.E., Holden, J.F., McDuff, R.E., Lilley, M.D., Delaney, J.R., 1997. Seafloor eruptions and evolution of hydrothermal fluid chemistry. *Philos. Trans. R. Soc. Lond. A.* **355**, 369–386.

Butterfield, D.A., Nelson, B.K., Wheat, G.W., Mottl, M.J., Roe, K.K., 2001. Evidence for basaltic Sr in mid-ocean ridge-flank hydrothermal

systems and implications for the global oceanic Sr isotope balance. *Geochim. Cosmochim. Acta* **65**, 4141–4153.

Canales, J.P., Tucholke, B.E., Collins, J.A., 2004. Seismic reflection imaging of an oceanic detachment fault: Atlantis Megamullion (Mid-Atlantic Ridge, 30°10′N). *Earth Planet. Sci. Lett.* **222**, 543–560.

Cann, J.R., Blackman, D.K., Smith, D.K., McAllister, E., Janssen, B., Mello, S., Avgerinos, E., Pascoe, A.R., Escartin, J., 1997. Corrugated slip surfaces formed at ridge-transform intersections on the Mid-Atlantic Ridge. *Nature* **385**, 329–330.

Charlou, J.L., Donval, J.P., Fouquet, Y., Jean-Baptiste, P., Holm, N., 2002. Geochemistry of high H_2 and CH_4 vent fluids issuing from ultramafic rocks at the Rainbow hydrothermal field (36°14′N, MAR). *Chem. Geol.* **191**, 345–359.

Cortesogno, L., Galbiati, B., Principi, G., 1981. Descrizione dettagliata di alcuni caratteristici affioramenti di brecce serpentinitiche della Liguria orientale ed interpretazione in chiave geodinamica. *Ofioliti* **6**, 47–76.

Council, T.C., Bennett, P.C., 1993. Geochemistry of ikaite formation at Mono Lake, California: implications for the origin of tufa mounds. *Geology* **21**, 971–974.

Delaney, J.R., Robigou, V., McDuff, R.E., 1992. Geology of a Vigorous hydrothermal system on the Endeavor Segment, Juan de Fuca Ridge. *J. Geophys. Res.* **97**, 19663–19682.

Desmurs, L., Manatschal, G., Bernoulli, D., 2001. The Steinmann Trinity revisited: mantle exhumation and magmatism along an ocean-continent transition. In: Wilson, R.C.L., Whitmarsh, R.B., Taylor, B., Froitzheim, N. (Eds.), *Non-volcanic Rifting of Continental Margins: A Comparison of Evidence from Land and Sea*, 187. Geological Society of London Special Publication, London, pp. 235–266.

Douville, E., Charlou, J.L., Oelkers, E.H., Bienvenu, P., Jove Colon, C.F., Donval, J.P., Fouquet, Y., Prieur, D., Appriou, P., 2002. The Rainbow vent fluids (36°14′N, MAR): the influence of ultramafic rocks and phase separation on trace metal content in Mid-Atlantic Ridge hydrothermal fluids. *Chem. Geol.* **184**, 37–48.

Edmonds, H.N., Michael, P.J., Baker, E.T., Connelly, D.P., Snow, J.E., Langmuir, C.H., Dick, H.J.B., Mühe, R., German, C.R., Graham, D.W., 2003. Discovery of abundant hydrothermal venting on the ultraslow-spreading Gakkel ridge in the Arctic Ocean. *Nature* **421**, 252–256.

Fouquet, Y., Wafik, A., Cambon, P., Mevel, C., Meyer, G., Gente, P., 1993. Tectonic setting and mineralogical and geochemical zonation in the Snake Pit sulfide deposit (Mid-Atlantic Ridge at 23°N). *Econ. Geol.* **88**, 2018–2036.

Fouquet, Y., Charlou, J.L., Ondreas, H., Radford-Knoery, J., Donval, J.P., Douville, E., Apprioual, R., Cambon, P., Pelle, H., Landure, J.Y., Normand, A., Ponzevera, E., German, C., Parson, L., Barriga, F., Costa, I., Relvas, J., Ribeiro, A., 1997. Discovery and first submersible investigations on the Rainbow hydrothermal field on the MAR (36°14′N). *Chem. Geol.* **184**, 37–48.

Früh-Green, G.L., Weissert, H., Bernoulli, D., 1990. A multiple fluid history recorded in Alpine ophiolites. *J. Geol. Soc. London* **147**, 959–970.

Früh-Green, G.L., Kelley, D.S., Bernasconi, S.M., Karson, J.A., Ludwig, K.A., Butterfield, D.A., Boschi, C., Proskurowski, G., 2003. 30,000 years of hydrothermal activity at the Lost City vent field. *Science* **301**, 495–498.

Fryer, P., 1996. Tectonic evolution of the Mariana convergent margin. *Rev. Geophys.* **34** (1), 89–125.

Fryer, P., Saboda, K.L., Johnson, L.E., Mackay, M.E., Moore, G.F., Stoffers, P., 1990. Conical Seamount: SeaMARC II, Alvin submersible and seismic reflection studies. In: *Proceedings of the Ocean Drilling Program, Initial Reports*, **125**, 69–80.

Fryer, P., Wheat, C.G., Mottl, M.J., 1999. Mariana blueschist mud volcanism: implications for conditions within the subduction zone. *Geology* **27**, 103–106.

Gracia, E., Charlou, J.L., Radford-Knoery, J., Parson, L.M., 2000. Non-transform offsets along the Mid-Atlantic Ridge south of the Azores (38°N–34°N): ultramafic exposures and hosting of hydrothermal vents. *Earth Planet. Sci. Lett.* **177**, 89–103.

Haggerty, J.A., 1987. Petrology and geochemistry of Neogene sedimentary rocks from Mariana Forearc seamounts: implications for emplacement of the seamounts. In: Keating, B.H., Fryer, P., Batiza, R., Boehlert, G.W. (Eds.), *Seamounts, Islands, and Atolls*. American Geophysical Union, Washington, DC, pp. 175–185.

Haggerty, J.A., 1991. Evidence from fluid seeps atop serpentine seamounts in the Mariana Forearc: clues for emplacement of the seamounts and their relationship to forearc tectonics. *Mar. Geol.* **102**, 293–309.

Hannington, M.D., Jonasson, I.R., Herzig, P.M., Petersen, S., 1995. Physical and chemical processes of seafloor mineralization at mid-ocean ridges. In: Humphris, S.E., Zierenberg, R.A., Mullineaux, L.S., Thomson, R.E. (Eds.), *Seafloor Hydrothermal Systems: Physical, Chemical, Biological, and Geological Interactions*. American Geophysical Union, Washington, DC, pp. 115–157.

Hopkinson, L., Beard, J.S., Boulter, C.A., 2004. The hydrothermal plumbing of a serpentinite-hosted detachment: evidence from the West Iberia non-volcanic rifted continental margin. *Mar. Geol.* **204**, 301–315.

IODP Expedition Scientific Party, 2005. Oceanic core complex formation, Atlantis Massif—oceanic core complex formation, Atlantis Massif, Mid-Atlantic Ridge: drilling into the footwall and hanging wall of a tectonic exposure of deep, young oceanic lithosphere to study deformation, alteration, and melt generation. *IODP Prel. Rept.*, **304**, doi:10.2204/iodp.pr.304.2005.

IODP Expedition Scientific Party, 2005. Oceanic core complex formation, Atlantis Massif—oceanic core complex formation, Atlantis Massif, Mid-Atlantic Ridge: drilling into the footwall and hanging wall of a tectonic exposure of deep, young oceanic lithosphere to study deformation, alteration, and melt generation. *IODP Prel. Rept.*, **305**, doi:10.2204/iodp.pr.305.2005.

Johannes, W., Metz, P., 1968. Experimental determinations of the equilibrium relations in the system $MgO–CO_2–H_2O$. *Neues Jb. Miner. Monat.* **16**, 15–26.

Kahmi, S.R., 1963. On the structure of vaterite, $CaCO_3$. *Acta Cryst.* **16**, 770–772.

Karson, J.A., Williams, E.A., Früh-Green, G.L., Kelley, D.S., Yoerger, D.R., Jakuba, M., 2006. Detachment Shear Zone of the Atlantis Massif Core Complex, Mid-Atlantic Ridge 30°N, *Geochem. Geophys. Geosys.*, **7**, in press.

Kelley, D.S., Karson, J.A., Blackman, D.K., Früh-Green, G.L., Butterfield, D.A., Lilley, M.D., Olson, E., Schrenk, M.O., Roe, K., Lebon, G.T., Rivissigno, P., the AT3-60 Shipboard Party, 2001. An off-axis hydrothermal vent field near the Mid-Atlantic Ridge at 30°N. *Nature* **412**, 145–149.

Kelley, D.S., Karson, J.A., Früh-Green, G.L., Yoerger, D., Shank, T.M., Butterfield, D.A., Hayes, J.M., Schrenk, M.O., Olson, E., Proskurowski, G., Jakuba, M., Bradley, A., Larson, B., Ludwig, K., Glickson, D., Buckman, K., Bradley, A.S., Brazelton, W.J., Roe, K., Elend, M.J., Delacour, A., Bernasconi, S.M., Lilley, M.D., Baross, J.A., Summons, R.E., Sylva, S.P., 2005. A Serpentinite-hosted ecosystem: the lost city hydrothermal field. *Science* **307**, 1428–1434.

Krasnov, S.G., Cherkashev, G.A., Stepanova, T.V., Batuyev, B.N., Krotov, A.G., Malin, B.V., Maslov, M.N., Markov, V.F., Poroshina, I.M., Samovarov, M.S., Ashadze, A.M., Lazareva, L.I., Ermolayev, I.K., 1995. Detailed geological studies of hydrothermal fields in the North Atlantic. In: Parson, L.M., Walker, C.L., Dixon, D.R. (Eds.), *Hydrothermal Vents and Processes*, No. 87. Geological Society Special Publication, pp. 43–64.

Lemoine, M., 1980. Serpentinites, gabbros and ophicalcites in the Piemont-Ligurian domain of the Western Alps: possible indicators of oceanic fracture zones and of associated serpentinite protrusions in the Jurassic-Cretaceous Tethys. *Archives des Science Genève* **33**, 105–115.

Marland, G., 1975. The stability of $CaCO_3{\cdot}6H_2O$ (ikaite). *Geochim. Cosmochim. Acta* **39**, 83–91.

Milliken, K.L., Morgan, J.K., 1996. Chemical evidence for near-seafloor precipitation of calcite in serpentinites (site 897) and serpentinite breccias (site 899), Iberia Abyssal Plain. In: *Proceedings of the Ocean Drilling Program, Scientific Results* **149**, 553–558.

Moody, J.B., 1976. Serpentinization: a review. *Lithos* **9**, 125–138.

Morford, J.L., Emerson, S., 1999. The geochemistry of redox sensitive trace metals in sediments. *Geochim. Cosmochim. Acta* **63**, 1735–1750.

Morgan, J.K., Milliken, K.L., 1996. Petrography of calcite veins in serpentinized peridotite basement rocks from the Iberia Abyssal Plain, sites 897 and 899: kinematic and environmental implications. In: *Proceedings of the Ocean Drilling Program, Scientific Results*, **149**, 559–569.

Mottl, M.J., 1992. Pore waters from serpentinite seamounts in the Mariana and Izu-Bonin forearcs, Leg 125: evidence for volatiles from the subducting slab. In: *Proceedings of the Ocean Drilling Program, Science Results*, **125**, 373–386.

Mottl, M.J., Wheat, C.G., 1994. Hydrothermal circulation through mid-ocean ridge flanks: fluxes of heat and magnesium. *Geochim. Cosmochim. Acta* **58**, 2225–2237.

Mottl, M.J., Komor, S.C., Fryer, P., Moyer, C.L., 2003. Deep-slab fluids fuel extremophilic Archaea on a Mariana forearc serpentinite mud volcano: Ocean Drilling Program Leg 195. *Geochem. Geophys. Geosys.* **4** (11). doi:10.1029/2003GC000588.

Mottl, M.J., Wheat, C.G., Fryer, P., Gharib, J., Martin, J.B., 2004. Chemistry of springs across the Mariana forearc shows progressive devolatilization of the subducting plate. *Geochim. Cosmochim. Acta* **68**, 4915–4933.

Nelson, B.K., 1995. Fluid flow in subduction zones: evidence from Nd- and Sr-isotope variations in metabasalts of the Franciscan complex, California. *Contrib. Mineral. Petrol.* **119**, 247–262.

O'Hanley, D.S., 1996. *Serpentinites: Records of Tectonic and Petrological History*. Oxford University Press, New York.

Palandri, J.L., Reed, M.H., 2004. Geochemical models of metasomatism in ultramafic systems: serpentinization, rodingitization, and sea floor carbonate chimney precipitation. *Geochim. Cosmochim. Acta* **68**, 1115–1133.

Palmer, M.R., 1992. Controls over the chloride concentration of submarine hydrothermal vent fluids: evidence from Sr/Ca and $^{87}Sr/^{86}Sr$ ratios. *Earth Planet. Sci. Lett.* **109**, 37–46.

Palmer, M.R., Edmond, J.M., 1989. The strontium isotope budget of the modern ocean. *Earth Planet. Sci. Lett.* **92**, 11–26.

Pauly, H., 1963. "Ikaite," a new mineral from Greenland. *Arctic* **16**, 263–264.

Pilson, M.E.Q., 1998. *An Introduction to the Chemistry of the Sea*. Prentice Hall, New Jersey.

Proskurowski, G., Lilley, M.D., Kelley, D.S., Olson, E.J., 2006. Low temperature volatile production at the Lost City Hydrothermal Field, evidence from a hydrogen stable isotope geothermometer. *Chem. Geol.* **229**, 331–343.

Pytkowicz, R.M., 1973. Calcium carbonate retention in supersaturated seawater. *Am. J. Sci.* **273**, 515–522.

Rimstidt, J.D., Balog, A., Webb, J., 1998. Distribution of trace elements between carbonate minerals and aqueous solutions. *Geochim. Cosmochim. Acta* **62**, 1851–1863.

Rona, P.A., Windenfalk, L., Bostrom, K., 1987. Serpentinized ultramafics and hydrothermal activity at the Mid-Atlantic Ridge Crest near 15°N. *J. Geophys. Res.* **92**, 1417–1427.

Schroeder, T., John, B.E., 2004. Strain localization on an oceanic detachment fault system, Atlantis Massif, 30°N, Mid-Atlantic Ridge. *Geochem. Geophys. Geosys.* **5**. doi:10.1029/2004GC000728.

Seyfried, W.E., Foustoukos, D.J., Allen, D.E., 2004. Ultramafic-hosted hydrothermal systems at Mid-ocean ridges: chemical and physical controls on pH, redox, and carbon reduction reactions. In: German, C., Lin, J., Parson, L.M. (Eds.), *Mid-Ocean Ridges: Hydrothermal Interactions between the Lithosphere and Oceans*. American Geophysical Union, Washington, DC, pp. 267–284.

Shearman, D.J., McGugan, A., Stein, C., Smith, A.J., 1989. Ikaite, $CaCO_3{\cdot}6H_2O$, precursor of the thinolites in the Quaternary tufas and tufa mounds of the Lahontan and Mono Lake Basins, western United States. *Geol. Soc. Am. Bull.* **101**, 913–917.

Smith, D.K., Escartin, J., Cannat, M., Tolstoy, M., Fox, C.G., Bohnenstiehl, D.R., Bazin, S., 2003. Spatial and temporal distribution of seismicity along the northern Mid-Atlantic Ridge (15–35°N). *J. Geophys. Res.* **108**, 31.

Teagle, D.A.H., Alt, J.C., Chiba, H., Humphris, S.E., Halliday, A.N., 1998. Strontium and oxygen isotopic constraints on fluid mixing, alteration, and mineralization in the TAG hydrothermal deposit. *Chem. Geol.* **149**, 1–24.

Treves, B.E., Harper, G.D., 1994. Exposure of serpentinites on the ocean floor: sequence of faulting and hydrofracturing in the northern Apennine ophicalcites. *Ofioliti* **19b**, 435–466.

Treves, B., Hickmott, D., Vaggelli, G., 1995. Texture and microchemical data of oceanic hydrothermal calcite veins, northern Apennine ophicalcites. *Ofioliti* **20**, 111–122.

Vecht, A., Ireland, T.G., 2000. The role of vaterite and aragonite in the formation of pseudo-biogenic carbonate structures: implications for Martian exobiology. *Geochim. Cosmochim. Acta* **64**, 2719–2725.

Veizer, J., 1983. Trace elements and isotopes in sedimentary carbonates. In: Reeder-Richard, J. (Ed.), *Carbonates; Mineralogy and chemistry*. Mineralogical Society of America, Washington, DC, pp. 265–299.

Von Damm, K., 1995. Controls on the chemistry and temporal variability of seafloor hydrothermal fluids. In: Humphris, S.E., Zierenberg, R.A., Mullineaux, L.S., Thomson, R.E. (Eds.), *Seafloor Hydrothermal Systems: Physical, Chemical, Biological, and Geological interactions*. American Geophysical Union, Washington, DC, pp. 222–247.

Von Damm, K., 2000. Chemistry of hydrothermal vent fluids from 9°–10°N, East Pacific Rise; "time zero," the immediate posteruptive period. *J. Geophys. Res.* **105**, 11203–11222.

Weissert, H.J., Bernoulli, D., 1984. Oxygen isotope composition of calcite in Alpine ophicarbonates: a hydrothermal or Alpine metamorphic signal? *Eclogae gelogicae Helvetiae* **77**, 29–43.

Weissert, H.J., Bernoulli, D., 1985. Transform margin in the Meoszoic Tethys: evidence from the Swiss Alps. *Geol. Rundschau* **74**, 665–679.

Wheat, C.G., Mottl, M.J., 2000. Composition of pore and spring waters from Baby Bare; global implications of geochemical fluxes from a ridge flank hydrothermal system. *Geochim. Cosmochim. Acta* **64**, 629–642.